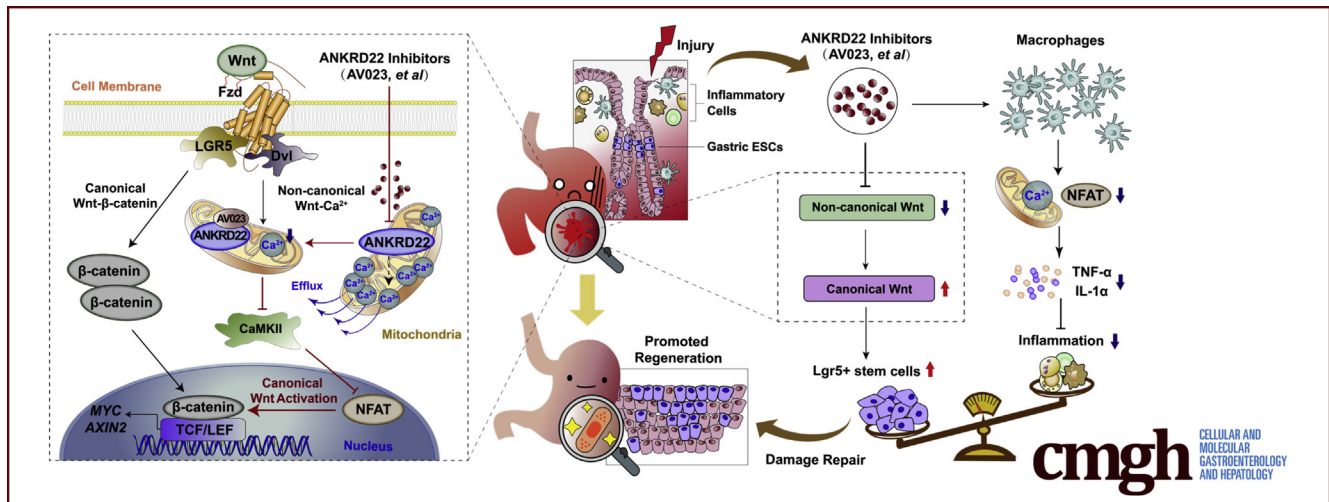


## ORIGINAL RESEARCH

ANKRD22 Drives Rapid Proliferation of Lgr5<sup>+</sup> Cells and Acts as a Promising Therapeutic Target in Gastric Mucosal Injury

Jingwen Liu,<sup>1,\*</sup> Jingni Wu,<sup>1,\*</sup> Rui Wang,<sup>1</sup> Dandan Zhong,<sup>1</sup> Yiqing Qiu,<sup>2</sup> Hongping Wang,<sup>1</sup> Zhenya Song,<sup>3,§</sup> and Yongliang Zhu<sup>1,4,§</sup>

<sup>1</sup>Laboratory of Gastroenterology, <sup>2</sup>Department of Urology Surgery, <sup>3</sup>Department of International Healthcare Center and General Medicine, Second Affiliated Hospital of Zhejiang University School of Medicine, Hangzhou, Zhejiang, China; <sup>4</sup>Key Laboratory of Tumor Microenvironment and Immune Therapy of Zhejiang Province, Hangzhou, Zhejiang, China



## SUMMARY

Ankyrin repeat domain 22 inhibition drives the rapid proliferation of leucine-rich repeat-containing G-protein-coupled receptor 5-positive gastric epithelium progenitor cells and alleviates the inflammatory response after gastric mucosal damage. Ankyrin repeat domain 22 is an ideal therapeutic target and its inhibitory compound may be used for the target-based development of drugs.

**BACKGROUND & AIMS:** Rapid gastric epithelial progenitor cell (EPC) proliferation and inflammatory response inhibition play key roles in promoting the repair of gastric mucosal damage. However, specific targets inducing these effects are unknown. In this study, we explored the effects of a potential target, Ankyrin repeat domain 22 (ANKRD22).

**METHODS:** An acute gastric mucosal injury model was established with *Ankrd22*<sup>-/-</sup> and *Ankrd22*<sup>+/+</sup> mice by intragastric administration of acidified ethanol. Organoid culture and flow cytometry were performed to evaluate the effects of ANKRD22 on leucine-rich repeat-containing G-protein-coupled receptor 5-positive (Lgr5<sup>+</sup>) gastric EPC proliferation. The mechanisms by which ANKRD22 affects gastric EPC proliferation and inflammatory responses were explored by mitochondrial Ca<sup>2+</sup>

influx and immunoblotting. Candidate ANKRD22 inhibitors then were screened virtually and validated in vitro and in vivo.

**RESULTS:** After acute gastric mucosal injury, the number of Lgr5<sup>+</sup> gastric EPCs was increased significantly in *Ankrd22*<sup>-/-</sup> mice compared with that in *Ankrd22*<sup>+/+</sup> mice. Moreover, *Ankrd22* knockout attenuated inflammatory cell infiltration into damaged gastric tissues. ANKRD22 deletion also reduced mitochondrial Ca<sup>2+</sup> influx and cytoplasmic nuclear factor of activated T cells in gastric epithelial cells and macrophages, which further induced Lgr5<sup>+</sup> gastric EPC proliferation and decreased macrophage release of tumor necrosis factor-α and interleukin 1α. In addition, a small molecule, AV023, was found to show similar effects to those produced by ANKRD22 deletion in vitro. Intraperitoneal injection of AV023 into the mouse model promoted the repair of gastric mucosal damage, with increased proliferation of Lgr5<sup>+</sup> gastric EPCs and visible relief of inflammation.

**CONCLUSIONS:** ANKRD22 inhibition is a potential target-based therapeutic approach for promoting the repair of gastric mucosal damage. (*Cell Mol Gastroenterol Hepatol* 2021;12:1433–1455; <https://doi.org/10.1016/j.jcmgh.2021.06.020>)

**Keywords:** Gastric Mucosal Injury; ANKRD22; Epithelial Progenitor Cells; Inhibitory Compound.

The unique location and functional characteristics of the stomach make the gastric mucosa very prone to damage. This damage may lead to gastric mucosal erosion, bleeding, and even ulcers, which are associated closely with the occurrence of gastric cancer.<sup>1,2</sup> High levels of gastric acid, alcohol consumption, use of nonsteroidal anti-inflammatory drugs, and *Helicobacter pylori* infection are the common causes of gastric mucosal damage.<sup>3,4</sup> In addition to reducing or avoiding exposure to injury-related factors, repairing the damaged gastric mucosa quickly and effectively is essential to maintaining the integrity of the gastric mucosal barrier.

Gastric epithelial progenitor cells (EPCs), in particular the leucine-rich repeat-containing G-protein-coupled receptor 5-positive (Lgr5<sup>+</sup>) EPCs, play a critical role in the rapid repair of damaged gastric mucosal epithelium. These progenitor cells are located in the isthmus and basal region of the gastric glands and drive the regeneration of the gastric epithelium.<sup>5,6</sup> Lineage tracking has shown that when the gastric mucosa is injured, the Wingless/Int1 (Wnt) pathway is up-regulated and quickly activates the Lgr5<sup>+</sup> EPCs to promote mucosal repair.<sup>7-9</sup> However, proliferation of Lgr5<sup>+</sup> gastric EPCs is hindered by the inflammatory microenvironment that the damage creates.

The formation of an inflammatory microenvironment occurs with activation of the macrophages, which play important roles in the mediation of the inflammatory cascades and activation of the immune cells when the gastric mucosa is injured.<sup>10,11</sup> Proinflammatory factors secreted by macrophages, such as interleukin-1 $\alpha$  (IL1 $\alpha$ ) and tumor necrosis factor- $\alpha$  (TNF- $\alpha$ ), can weaken the proliferation and differentiation of EPCs and hinder the regeneration and repair of the mucosa.<sup>12,13</sup> Therefore, the rapid proliferation of gastric EPCs and the inhibition of local inflammation are the key mechanisms responsible for promoting the repair of gastric mucosal damage.

Several agents, including the gastric mucosal protective agents, have been used recently in clinics to enhance the gastric mucosal barrier function to treat injuries.<sup>14</sup> However, the pharmacodynamic mechanisms of these agents depend mostly on the nonspecific neutralization of gastric acid and pain relief.<sup>15,16</sup> Sucralfate, bismuth potassium citrate, and Ecabet sodium commonly chelate the gastric mucosa to physically resist the damage caused by gastric acid, pepsin, and other harmful substances. Hydrotalcite, misoprostol, and teprenone act by promoting the secretion of mucus, epidermal growth factor, and other growth factors, which increase the gastric mucosal blood flow and inhibit the secretion of gastric acid as well as the activities of pepsins. However, these agents cannot induce rapid proliferation of gastric EPCs while reducing local inflammation because they do not possess precise drug targets. Therefore, it is necessary to develop novel agents that can promote the regeneration and repair of the mucosa for efficient treatment of gastric mucosal injury.

In previous studies using a patient-derived tumor xenograft mouse model and global complementary DNA

expression profile scanning, we identified a novel mitochondrial protein, ankyrin repeat domain-containing protein 22 (ANKRD22), which is induced by the tumor microenvironment to promote the reprogramming of colorectal cancer cells as well as the self-renewal of the colorectal cancer-initiating cells.<sup>17</sup> More importantly, pronounced expression of ANKRD22 can be observed in the normal human gastric epithelium, while increased expression is seen in the activated macrophages.<sup>18</sup> However, the specific function of ANKRD22 in the gastric epithelium remains unclear.

Here, we aimed to explore the role of ANKRD22 in the repair of gastric mucosal damage. We found that suppression of ANKRD22 could promote proliferation of Lgr5<sup>+</sup> gastric EPCs, while reducing mucosal inflammation. Therefore, inhibition of ANKRD22 may be a promising therapeutic approach for the treatment of gastric mucosal barrier injury.

## Results

### *Expression of ANKRD22, a Mitochondrial Molecule That Is Widely Expressed in the Gastric Epithelium, Is Decreased After Mucosal Damage*

ANKRD22 was highly expressed in normal human gastric epithelium, as indicated by The Human Protein Atlas (Figure 1A). Thus, to verify the expression level of ANKRD22 in the gastric epithelium, we first detected ANKRD22 expression in the normal human gastric epithelium by immunohistochemistry (IHC) staining of human samples. ANKRD22 was widely expressed in the cytoplasm of cells in gastric pits and glands (Figure 1B). Consistent with the intestinal epithelium IHC results,<sup>17</sup> fluorescence colocalization in gastric SGC7901 and BGC823 cells indicated that exogenously expressed ANKRD22 was distributed almost completely in the mitochondria (Figure 1C). Western blot

\*Authors share co-first authorship; §Authors share co-senior authorship.

**Abbreviations used in this paper:** ANKRD22, ankyrin repeat domain-containing protein 22; AXIN2, axis inhibition protein 2; BrdU<sup>+</sup>, bromodeoxyuridine-incorporating; CaMKII, calmodulin-dependent protein kinase II; Cd, cluster of differentiation; c-Myc, Myc proto-oncogene protein; DMEM, Dulbecco's modified Eagle medium; ELISA, enzyme-linked immunosorbent assay; EPC, epithelial progenitor cell; FACS, fluorescence-activated cell sorting; FBS, fetal bovine serum; FCM, flow cytometry; FITC, fluorescein isothiocyanate; IFN- $\gamma$ , interferon- $\gamma$ ; IHC, immunohistochemistry; IL1 $\alpha$ , interleukin-1 $\alpha$ ; Lgr5<sup>+</sup>, leucine-rich repeat-containing G-protein-coupled receptor 5-positive; LPS, lipopolysaccharide; Mist, Muscle, intestine and stomach expression; mRNA, messenger RNA; NFAT, nuclear factor of activated T cells; PBS, phosphate-buffered saline; PE, Phycocerythrin; qRT-PCR, quantitative reverse-transcription polymerase chain reaction; Rhod-2, Dihydrorhod-2; RIPA, radioimmunoprecipitation assay; Sox, SRY-box transcription factor; Ssea, stage-specific embryonic antigen; TBS, Tris-buffered saline; THP-1, Human myeloid leukemia mononuclear cell; TNF- $\alpha$ , tumor necrosis factor  $\alpha$ ; Wnt, Wingless/Int1; WT, wild-type.

 Most current article

© 2021 The Authors. Published by Elsevier Inc. on behalf of the AGA Institute. This is an open access article under the CC BY-NC-ND license (<http://creativecommons.org/licenses/by-nc-nd/4.0/>).

2352-345X

<https://doi.org/10.1016/j.jcmgh.2021.06.020>

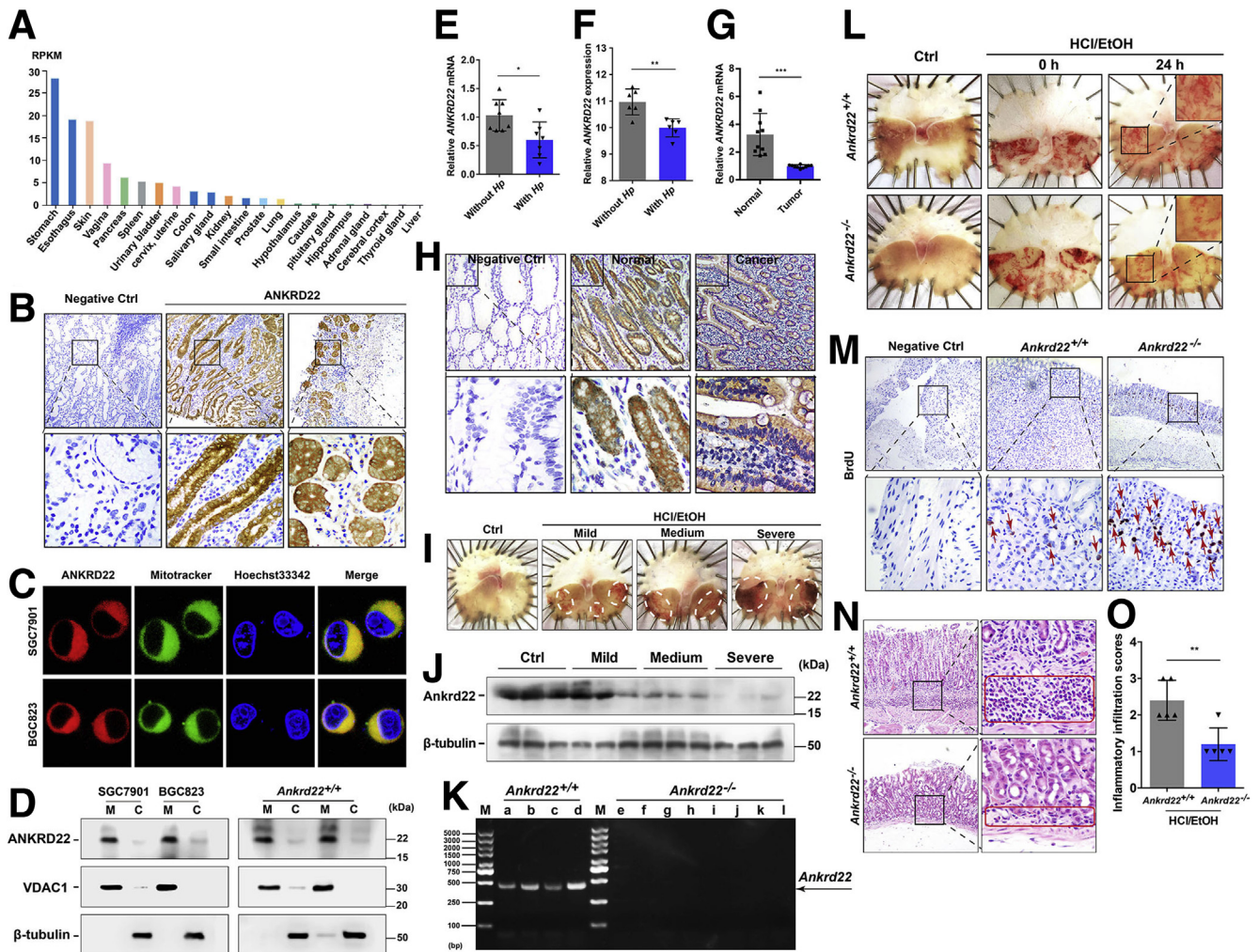


**Figure 1.** The expression of ANKRD22, a mitochondrial molecule that is widely expressed in the gastric epithelium, is decreased after mucosal damage. (A) Expression levels of ANKRD22 in different tissues of the human body. Analysis was performed using The Human Protein Atlas (<https://www.proteinatlas.org/ENSG00000152766-ANKRD22/tissue>) data, of which the RNA sequencing expression data were from the Genotype-Tissue Expression (GTEx) projects. (B) Expression of ANKRD22 in the human normal gastric epithelium detected by IHC staining. Normal mouse IgG was used as negative control. (C) Mitochondrial colocalization of the exogenous-expressing ANKRD22 in gastric cancer cells detected by confocal microscopy. (D) Detection of ANKRD22 in the mitochondria (M) and a residual cytoplasmic fraction (C) of cells exogenous expressing ANKRD22 and WT C57BL/6 mouse gastric tissues by Western blot. Voltage-dependent anion channel 1 (VDAC1) and  $\beta$ -tubulin were internal references for the mitochondrial and cytoplasmic fractions, respectively. (E) Expression levels of ANKRD22 in the human gastric tissues with *H pylori* infection ( $n = 8$ ) and those without *H pylori* infection ( $n = 8$ ) as determined by qRT-PCR. The data from the non-*H pylori* group were normalized to 1.0. Tubulin  $\beta$  class I (*TUBB*) was used as an internal reference. (F) Expression levels of ANKRD22 in the human gastric tissues with *H pylori* infection ( $n = 6$ ) and normal epithelial tissues without *H pylori* infection ( $n = 6$ ) in 2 data sets (ID: 125281861 and 122519261) from the Gene Expression Omnibus profiles database. (G) Expression levels of ANKRD22 in human gastric cancer tissues and corresponding adjacent noncancerous tissues in gastric cancer patients ( $n = 10$ ) determined by qRT-PCR. *TUBB* was used as an internal reference. (H) Expression levels of ANKRD22 in human normal and cancerous gastric epithelium detected by IHC staining. Normal mouse IgG was used as a negative control (Ctrl). (I) Representative macroscopic view of the mouse gastric mucosa with different degrees of damage. WT C57BL/6 mice were observed at 24 hours after intragastric administration of EtOH/HCl or saline solution (Ctrl) ( $n = 3$ ). (J) Detection of ANKRD22 in mouse gastric mucosa with different degrees of damage by Western blot ( $n = 3$ ). (K) Validation of ANKRD22 in the gastric tissues of *Ankrd22*<sup>+/+</sup> ( $n = 4$ ) and *Ankrd22*<sup>-/-</sup> ( $n = 8$ ) mice by PCR and agarose gel electrophoresis. M, marker. (L) *Ankrd22* knockout alleviated gastric mucosal injury in mice. After intragastric administration of EtOH/HCl or saline solution (Ctrl) and observation for 2 hours in advance, the *Ankrd22*<sup>+/+</sup> and *Ankrd22*<sup>-/-</sup> mice subsequently were checked at 0 or 24 hours ( $n = 3$ ). (M) *Ankrd22* knockout promoted cell proliferation in the injured mouse gastric mucosa as detected by IHC staining. Normal mouse IgG was used as a negative control. Arrow, BrdU<sup>+</sup> cells. (N and O) Effect of *Ankrd22* knockout on the inflammatory cell infiltration in the damaged mouse gastric mucosa as detected by H&E staining ( $n = 5$ ). Red square, inflammatory cell infiltration area. Data are presented as means  $\pm$  SD and analyzed by the Student *t* test. \**P* < .05, \*\**P* < .01, and \*\*\**P* < .001. *Hp*, *H pylori*; RPKM, Reads Per Kilobase per Million mapped reads.

showed that both exogenous and endogenous ANKRD22 were located in purified mitochondria from gastric cancer cells and wild-type C57BL/6 mice gastric tissues. (Figure 1D). These results suggest that the mitochondrial molecule ANKRD22 is widely expressed in the gastric epithelium, indicating a functional role in the stomach.

To explore the role of ANKRD22 in gastric disease status, quantitative reverse-transcription polymerase chain reaction (qRT-PCR) was used to detect the expression of ANKRD22 in patients with *H pylori* infection. The expression of ANKRD22 was slightly lower than that in paired normal epithelium in the absence of infection (Figure 1E). These findings were consistent with the results of Gene Expression Omnibus profile data analysis (Figure 1F). IHC staining and qRT-PCR analyses indicated that ANKRD22 expression was lower in human gastric cancer tissues than in the paired adjacent noncancerous tissues (Figure 1G and H), suggesting that ANKRD22 down-regulation is a common step in gastric pathogenic processes.

Next, we aimed to explore the changes in ANKRD22 under gastric epithelial stress by simulating mucosal injury to different degrees with EtOH/HCl solutions in wild-type (WT) C57BL/6 mice (Figure 1J), because ANKRD22 also was highly expressed in the normal gastric mucosa of mice. Western blot showed that ANKRD22 expression was substantially lower in damaged gastric mucosa after intragastric administration of various concentrations of acidified ethanol than in the normal gastric epithelium after administration of saline solution (Figure 1J). To further explore the relationship between ANKRD22 level and gastric mucosal injury, an *Ankrd22*<sup>-/-</sup> mouse strain was established using the clustered regularly interspaced short palindromic repeats/nuclease Cas9 technology (Figure 1K). Mild-to-moderate gastric mucosal damage was established in the mice to approximate clinical stress injuries. After 24 hours of intragastric administration of the EtOH/HCl solution (60% EtOH in 150 mmol/L HCl), the gastric mucosal damage in *Ankrd22*<sup>-/-</sup> mice was less severe than that in corresponding *Ankrd22*<sup>+/+</sup> mice (Figure 1L). Furthermore, IHC staining showed that the number of bromodeoxyuridine-incorporating cells (BrdU<sup>+</sup> cells) was increased notably in the gastric epithelium of *Ankrd22*<sup>-/-</sup> mice (Figure 1M), while H&E staining showed significantly reduced inflammatory cell infiltration in the *Ankrd22*<sup>-/-</sup> mouse gastric epithelium (Figure 1N and O). These results suggest the possible involvement of ANKRD22 in the gastric epithelial stress response in the repair of gastric mucosal damage and that ANKRD22 deletion promotes cell proliferation and reduces inflammation in the context of gastric mucosal damage.

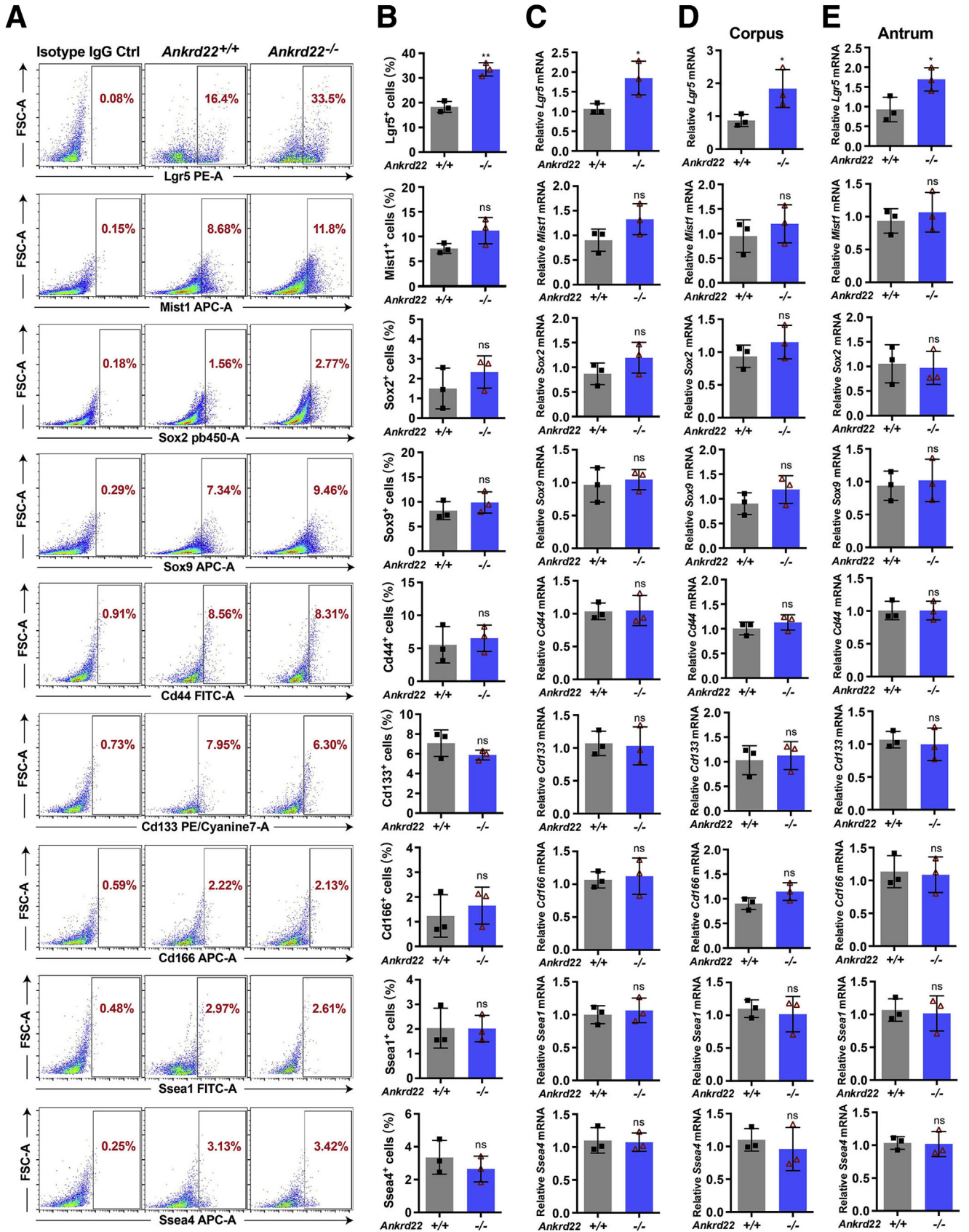
### ANKRD22 Deletion Results in Rapid Proliferation of Lgr5<sup>+</sup> Gastric EPCs

The results of BrdU incorporation suggest that ANKRD22 deletion could promote gastric epithelial cell proliferation in the context of gastric mucosal damage, thus prompting an experiment to determine the identity of these proliferating

cells by assessing gastric stemness-related markers, including Lgr5, Muscle, intestine and stomach expression 1 (Mist1), SRY-box transcription factor 2 (Sox2), Sox9, Troy, cluster of differentiation (Cd)-44, Cd133, Cd166, stage-specific embryonic antigen 1 (Ssea1), and Ssea4. Flow cytometry (FCM) analysis showed a significant increase in the prevalence of Lgr5<sup>+</sup> cells in *Ankrd22*<sup>-/-</sup> mice 24 hours after gastric mucosal injury compared with that in *Ankrd22*<sup>+/+</sup> mice (Figure 2A and B). Similarly, qRT-PCR showed significantly higher activity of *Lgr5* in cultured gastric epithelial organoids of *Ankrd22*<sup>-/-</sup> mice than *Ankrd22*<sup>+/+</sup> mice. No statistical difference was observed in the levels of the other markers (Figure 2C-E). These results suggest that the proliferating cells after ANKRD22 deletion were likely to be Lgr5<sup>+</sup> gastric EPCs. These are rapidly proliferating progenitor cells that maintain the gastric epithelium and repair mucosal damage by self-renewal and differentiation.<sup>7</sup>

To clarify the characteristics of Lgr5<sup>+</sup> cells in gastric mucosal injury, the gastric epithelial tissue of *Lgr5*-enhanced green fluorescent protein (EGFP)-internal ribosome entry site (IRES)-*creERT2* knockin mice was evaluated after intragastric administration of the EtOH/HCl solution. Lgr5<sup>+</sup> cells were notably enriched below the area of gastric mucosal damage compared with the noninjured area (Figure 3A). PCR showed that these Lgr5<sup>+</sup> cells obtained by fluorescent-activated cell sorting (FACS) also expressed different types of gastric epithelial markers similar to Lgr5<sup>+</sup> cells, including the gastric pit mucous marker mucin 5AC (*Muc5ac*), chief cell marker progastricsin (*Pgc*), endocrine cell marker somatostatin (*Sst*), gastric gland mucous cell markers mucin 6 (*Muc6*), trefoil factor 1 (*Tff1*), and *Tff2* (Figure 3B and C). These findings suggest that Lgr5<sup>+</sup> cells proliferating in the state of gastric mucosal injury possess the potential to differentiate into various types of gastric epithelial cells, which have the characteristics of gastric EPCs.

We further explored the effect of ANKRD22 on the proliferation of Lgr5<sup>+</sup> cells. qRT-PCR showed a marked increase in *Lgr5* messenger RNA (mRNA) levels in the gastric epithelium of *Ankrd22*<sup>-/-</sup> mice compared with those in *Ankrd22*<sup>+/+</sup> mice 24 hours after the stimulation of injury (Figure 3D). FCM analysis showed that the percentages of Lgr5<sup>+</sup> cells in *Ankrd22*<sup>-/-</sup> mice 24 and 48 hours after gastric mucosal injury were increased significantly compared with those in *Ankrd22*<sup>+/+</sup> mice (Figure 3E and F). Moreover, FCM indicated that *Ankrd22* knockout promoted the Lgr5<sup>+</sup> cell proliferation in both the corpus and antrum of injured gastric mucosal cells (Figure 3G and H). To determine the proliferation of Lgr5<sup>+</sup> cells in vitro after deletion of ANKRD22, we enriched the primary mouse gastric EPCs using an organoid culture. The number of organoid clones was significantly higher for the gastric epithelial cells of *Ankrd22*<sup>-/-</sup> mice than for *Ankrd22*<sup>+/+</sup> mice after stimulation of injury (Figure 3I). FCM showed that 30.7% of the cultured gastric epithelial organoids were enriched in Lgr5<sup>+</sup> EPCs. Of these, 59.3% were Lgr5<sup>+</sup>Ki67<sup>+</sup> proliferating cells (Figure 3J). Finally, we evaluated the relationship between the levels of ANKRD22 and *LGR5* in the gastric epithelium of patients with chronic gastritis by qRT-PCR. We found that the level of *LGR5* was



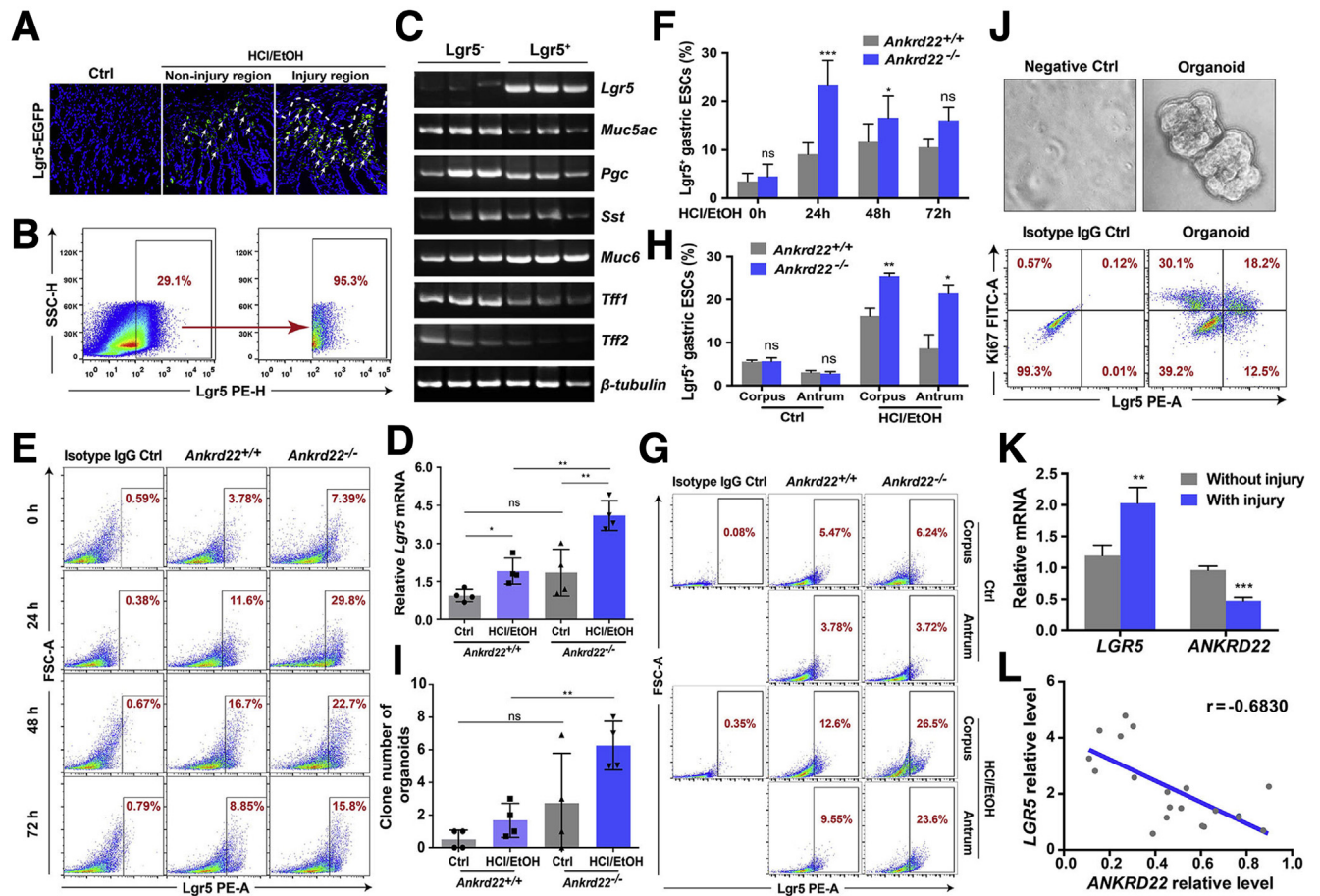


**Figure 3. ANKRD22 deletion results in rapid proliferation of the *Lgr5*<sup>+</sup> gastric EPCs.** (A) Detection of *Lgr5*<sup>+</sup> cells in injured gastric mucosa of *Lgr5-EGFP-IRES-creERT2* knockin mice. Mice were subjected to subsequent detection at 24 hours after intragastric administration of EtOH/HCl or saline solution (Ctrl). Arrow, *Lgr5*<sup>+</sup> cells. (B and C) Mucin 5AC (*Muc5ac*), progastriecin (*Pgc*), somatostatin (*Sst*), mucin 6 (*Muc6*), trefoil factor 1 (*Tff1*), and trefoil factor 2 (*Tff2*) were expressed in both *Lgr5*<sup>+</sup> and *Lgr5*<sup>-</sup> gastric epithelial cells detected by PCR. *Lgr5*<sup>+</sup> and *Lgr5*<sup>-</sup> gastric epithelial cells of WT C57BL/6 mice were obtained by FACS at 24 hours after intragastric administration of HCl/EtOH (n = 3). (D) Effect of *Ankrd22* knockout on *Lgr5* after gastric mucosal injury detected by qRT-PCR. The data from the *Ankrd22*<sup>+/+</sup> control group were normalized to 1.0. *TUBB* was used as an internal reference. (E and F) Effect of *Ankrd22* knockout on the percentage of *Lgr5*<sup>+</sup> cells after gastric mucosal injury detected by FCM. After intragastric administration of EtOH/HCl and observation for 2 hours in advance, *Ankrd22*<sup>+/+</sup> and *Ankrd22*<sup>-/-</sup> mice were examined at 0, 24, 48, or 72 hours. Rat IgG2b was used as isotype control (n = 5). (G and H) Effect of *Ankrd22* knockout on the percentage of *Lgr5*<sup>+</sup> cells in corpus and antrum after gastric mucosal injury detected by FCM. Rat IgG2b was used as an isotype control. (I) *Ankrd22* knockout increased the clone number of primary mouse gastric epithelial cells in organoid culture (n = 3). (J) The percentage of *Lgr5*<sup>+</sup>Ki67<sup>+</sup> cells in the organoid-enriched primary mouse gastric EPCs was detected by FCM. Rat IgG2b was used as an isotype control (n = 3). (K) Expression of *LGR5* and *ANKRD22* in human gastric epithelial mucosa with injury and corresponding mucosa without injury in chronic gastritis patients detected by qRT-PCR (n = 20). The data from the corresponding mucosa without injury group were normalized to 1.0. *TUBB* was used as an internal reference. (L) Correlation analysis of *LGR5* and *ANKRD22* in the gastric mucosal lesions in patients with chronic gastritis (n = 20). The data were analyzed by the Student *t* test and presented as means ± SD. \**P* < .05, \*\**P* < .01, and \*\*\**P* < .001. ESC, Epithelial Stem cells; FITC-A, Fluorescein Isothiocyanate Area; FSC-A, Forward Scatter Area; PE-A, Phycoerythrin Area; PE-H, Phycoerythrin Height; SSC-H, Side Scatter Height.

**Figure 2. (See previous page). Identification of the stemness markers in the proliferating cells after ANKRD22 deletion.** (A and B) Effects of *Ankrd22* knockout on the percentages of *Lgr5*<sup>+</sup>, *Mist1*<sup>+</sup>, *Sox2*<sup>+</sup>, *Sox9*<sup>+</sup>, *Troy*<sup>+</sup>, *Cd44*<sup>+</sup>, *Cd133*<sup>+</sup>, *Cd166*<sup>+</sup>, *Ssea1*<sup>+</sup>, and *Ssea4*<sup>+</sup> cells after gastric mucosal injury detected by FCM. Rat IgG2b was used as isotype control. (C-E) Effects of *Ankrd22* knockout on *Lgr5*, *Mist1*, *Sox2*, *Sox9*, *Cd44*, *Cd133*, *Cd166*, *Ssea1*, and *Ssea4* in organoid-enriched primary mouse gastric EPCs detected by qRT-PCR. The organoids were derived from the whole-mouse gastric tissue as well as the corpus and antrum. The data from the *Ankrd22*<sup>+/+</sup> group were normalized to 1.0. *TUBB* was used as an internal reference. (A-E) *Ankrd22*<sup>+/+</sup> and *Ankrd22*<sup>-/-</sup> mice were subjected to subsequent detection at 24 hours after intragastric administration of EtOH/HCl or saline solution (Ctrl) (n = 3). Data are presented as means ± SD and analyzed by the Student *t* test. \**P* < .05 and \*\**P* < .01. APC-A, Allophycocyanin Area; FITC-A, Fluorescein Isothiocyanate Area; FSC-A, Forward Scatter Area; PE-A, Phycoerythrin Area.

significantly higher in the injured mucosa than in the uninjured mucosa, while the expression of *ANKRD22* was reduced significantly in the uninjured mucosa (Figure 3K). The expression of *ANKRD22* was correlated negatively with the expression of *LGR5* in the gastric mucosal lesions of patients with chronic gastritis (Figure 3L). These results suggest that the loss of *ANKRD22* promotes rapid proliferation of the *Lgr5*<sup>+</sup> gastric EPCs in the context of gastric mucosal damage.

### *ANKRD22 Deletion Suppresses the Noncanonical Wnt-Ca<sup>2+</sup> Pathway*

The Wnt pathway plays critical roles in the proliferation of *Lgr5*<sup>+</sup> EPCs.<sup>19</sup> To study whether the effect of suppression of *ANKRD22* on the proliferation of *Lgr5*<sup>+</sup> EPCs is mediated via the Wnt pathway, we evaluated Wnt pathway activity in the mouse gastric tissues at 0, 24, 48, and 72 hours after EtOH/HCl-induced mucosal damage. Western blot showed that the expression levels of Myc proto-oncogene protein (c-Myc) and the axis inhibition protein 2 (AXIN2), the downstream targets of the Wnt pathway, were substantially higher in the gastric epithelium of *Ankrd22*<sup>-/-</sup> mice than in *Ankrd22*<sup>+/+</sup> mice (Figure 4A). Conversely, the levels of c-Myc and AXIN2 were decreased significantly in *ANKRD22*-expressing gastric cancer cells compared with those in the control cells infected with the corresponding null lentivirus (Figure 4B), suggesting that *ANKRD22* plays a role in the regulation of the Wnt pathway.

We previously reported that *ANKRD22* is not involved directly in the canonical Wnt- $\beta$ -catenin pathway, but results in an increase in the intracellular concentration of Ca<sup>2+</sup>, suggesting that *ANKRD22* may affect the canonical Wnt pathway via the noncanonical Wnt-Ca<sup>2+</sup> pathway for the repair of gastric mucosal damage.<sup>17</sup> To determine the relationship between the expression of *ANKRD22* and the Wnt-Ca<sup>2+</sup> pathway, we first examined the changes in the intracellular levels of Ca<sup>2+</sup> in *Ankrd22*<sup>-/-</sup> mice 24 hours after gastric mucosal injury using the Fluo-4 dye. The Ca<sup>2+</sup> levels were significantly lower in the gastric mucosal epithelial cells of *Ankrd22*<sup>-/-</sup> mice than in those of *Ankrd22*<sup>+/+</sup> mice (Figure 4C). Similarly, the intracellular Ca<sup>2+</sup> levels were increased significantly in *ANKRD22*-expressing gastric cancer cells compared with those in the control cells infected with the corresponding null lentivirus (Figure 4D). *ANKRD22* also localized to the mitochondria in organoid-enriched progenitor cells as determined by the fluorescence colocalization analysis (Figure 4E). To clarify the effects of *Ankrd22* knockout on Ca<sup>2+</sup> levels in mitochondria, Dihydrorhod-2 (Rhod-2) was used to stain the mitochondrial Ca<sup>2+</sup>. The mitochondrial Ca<sup>2+</sup> levels were notably lower in the gastric epithelium of *Ankrd22*<sup>-/-</sup> mice than in *Ankrd22*<sup>+/+</sup> mice 24 hours after gastric mucosal injury (Figure 4F and G). These findings suggest that the suppression of expression of *ANKRD22* in gastric epithelial cells in damaged mucosa results in a decrease in the levels of mitochondrial Ca<sup>2+</sup>.

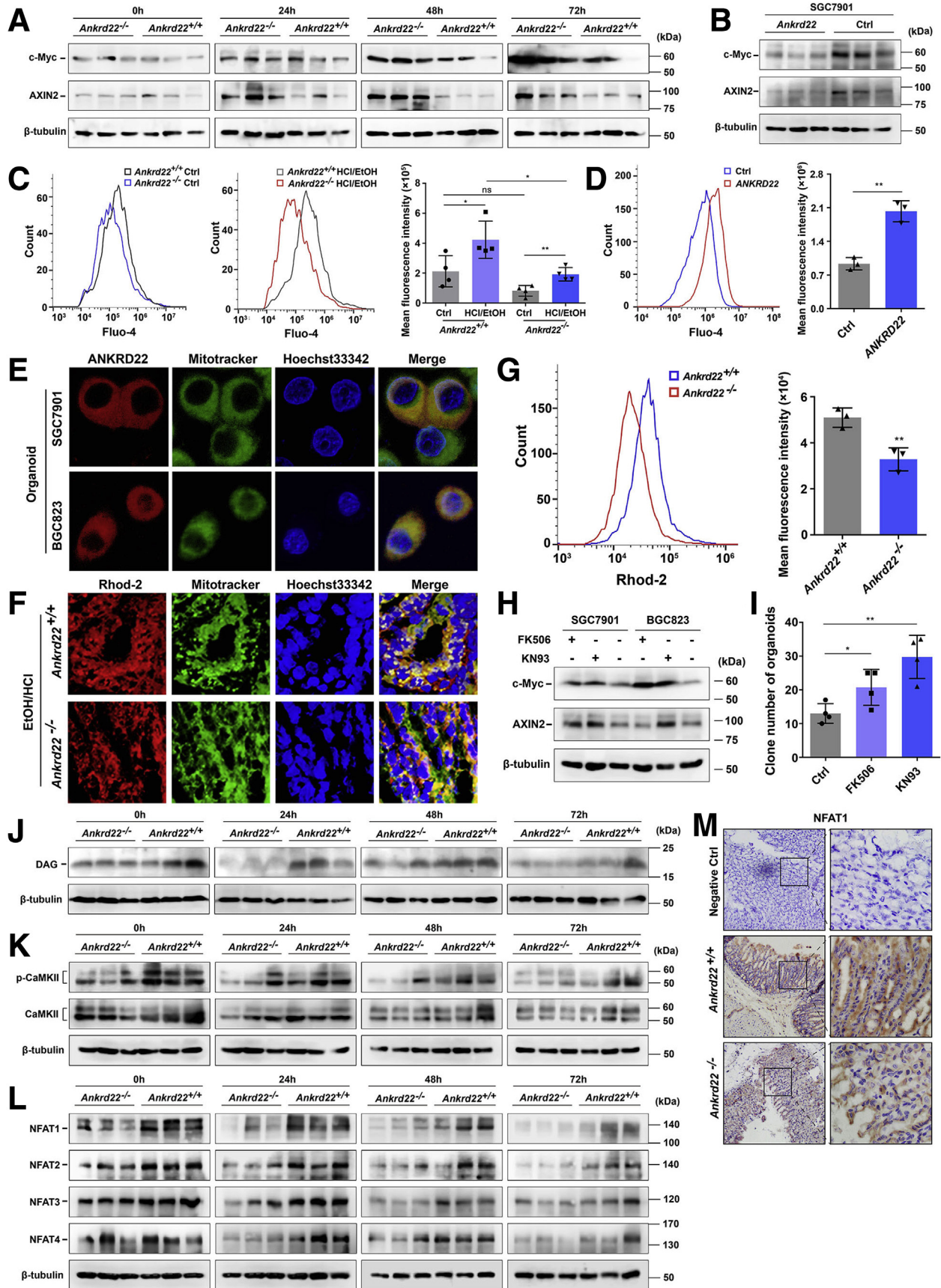
Next, to determine whether the Wnt-Ca<sup>2+</sup> pathway effectors can change the levels of the components of the canonical pathway, we used the nuclear factor of activated T

cells (NFAT) inhibitor, FK506, or the calmodulin-dependent protein kinase II (CaMKII) inhibitor, KN93, to treat cultured cells in vitro, because both NFAT and CaMKII lie downstream of the Wnt-Ca<sup>2+</sup> pathway. Western blot showed that the levels of c-Myc and AXIN2 were notably increased in treated cells (Figure 4H). The number of primary mouse gastric EPCs enriched by the organoid culture also was increased significantly after treatment with FK506 or KN93 (Figure 4I), suggesting that the activity of the canonical Wnt pathway was up-regulated after the inhibition of the Wnt-Ca<sup>2+</sup> pathway. Finally, the expression levels of the downstream targets in the Wnt-Ca<sup>2+</sup> pathway were detected in the mouse model of EtOH/HCl-induced gastric mucosal injury by Western blot. The expression levels of diacylglycerol, phosphorylated-CaMKII, and NFAT were reduced in the gastric epithelial cells of *Ankrd22*<sup>-/-</sup> mice at 0, 24, 48, and 72 hours after the stimulation of gastric mucosal injury compared with the levels observed in the gastric epithelial cells of *Ankrd22*<sup>+/+</sup> mice (Figure 4J-L). In addition, IHC staining showed that NFAT1 expression levels in the injured gastric mucosal cells were lower in *Ankrd22*<sup>-/-</sup> mice than in *Ankrd22*<sup>+/+</sup> mice (Figure 4M). These results suggest that the loss of *ANKRD22* inhibited the Wnt-Ca<sup>2+</sup> pathway, while indirectly up-regulating the activity of the canonical Wnt pathway, which may promote proliferation of the *Lgr5*<sup>+</sup> EPCs to aid in the repair of gastric mucosal damage.

### *ANKRD22 Deletion Reduces the Inflammatory Response by Inhibiting the Activation of Macrophages After Gastric Mucosal Injury*

The finding that inflammatory cell infiltration in the gastric epithelium of *Ankrd22*<sup>-/-</sup> mice was reduced significantly suggests that the deletion of *Ankrd22* reduced inflammation in gastric mucosal damage. To investigate the mechanism underlying this reduced inflammatory response in *Ankrd22*<sup>-/-</sup> mice, we examined changes in the proportions of inflammatory cells in the mouse gastric epithelium 24 hours after EtOH/HCl-induced mucosal injury. FCM showed that the percentage of CD45<sup>+</sup> leukocytes was significantly lower in the injured gastric epithelium of *Ankrd22*<sup>-/-</sup> mice than in *Ankrd22*<sup>+/+</sup> mice (Figure 5A and B). The Luminex (Austin, TX) assay and the enzyme-linked immunosorbent assay (ELISA) analyses showed significantly lower concentrations of TNF- $\alpha$  and IL1 $\alpha$  in injured gastric epithelium of *Ankrd22*<sup>-/-</sup> mice than those in *Ankrd22*<sup>+/+</sup> mice (Figure 5C-E), suggesting that the loss of *ANKRD22* alleviated gastric epithelium inflammation during gastric mucosal damage.

Macrophages play an important role in mediating inflammation in the context of gastric mucosal injury.<sup>10,11</sup> *ANKRD22* expression is increased in activated macrophages.<sup>18</sup> Therefore, we examined whether *ANKRD22* expression affects macrophage function. Human myeloid leukemia mononuclear cells (THP-1) were treated in advance with phorbol 12-myristate 13-acetate to induce macrophage function. qRT-PCR indicated that *ANKRD22* expression in both human THP-1 macrophages and mouse RAW264.7 macrophages was increased significantly in a dose-independent manner after stimulation with different



concentrations of interferon- $\gamma$  (IFN- $\gamma$ ) for 24 hours (Figure 5F). Likewise, after stimulating mouse peritoneal macrophages with 100 ng/mL lipopolysaccharide (LPS) for 24 hours, RT-PCR showed that *ANKRD22* expression in the activated macrophages was increased significantly (Figure 5G). The concentrations of TNF- $\alpha$  and IL1 $\alpha$  secreted by macrophages from *Ankrd22*<sup>-/-</sup> mice were significantly lower than those secreted by macrophages from *Ankrd22*<sup>+/+</sup> mice after stimulation with 50 ng/mL IFN- $\gamma$  or 100 ng/mL LPS for 24 hours, respectively (Figure 5H and I). The findings suggested that loss of ANKRD22 inhibited macrophage activation in gastric epithelial inflammation. We explored if ANKRD22 expression affected the polarization of macrophages. FCM showed an obvious reduction in the proportion of CD86<sup>+</sup> cells in activated *Ankrd22*<sup>-/-</sup> mouse macrophages compared with that in *Ankrd22*<sup>+/+</sup> mice, but no significant change in the number of CD206<sup>+</sup> cells (Figure 5J and K). Similarly, ELISA data showed significantly lower concentration of IL12 secreted by activated *Ankrd22*<sup>-/-</sup> mouse macrophages than that in *Ankrd22*<sup>+/+</sup> mice, with no significant difference in the concentration of IL10 (Figure 5L and M), suggesting that *ANKRD22* deletion inhibited M1 polarization of macrophages but had no effect on M2 polarization.

Given the observations that loss of ANKRD22 reduced the Ca<sup>2+</sup> level in the mitochondria and NFAT expression in gastric epithelial cells, and because fluorescence colocalization detection indicated that ANKRD22 also was localized in the mitochondria in macrophages (Figure 6A), we questioned whether ANKRD22 also could regulate the mitochondrial Ca<sup>2+</sup> level and NFAT expression in macrophages. To assess this, we first activated mouse macrophages in vitro with IFN- $\gamma$  or LPS, or treated them with the Ca<sup>2+</sup>-selective chelator 1,2-bis(o-aminophenoxy)ethane-N,N,N',N'-tetraacetic acid as a negative control and performed Rhod-2 fluorescence staining. The mitochondrial Ca<sup>2+</sup> level of *Ankrd22*<sup>-/-</sup> mouse macrophages was notably lower than that of *Ankrd22*<sup>+/+</sup> mouse macrophages (Figure 6B–E), suggesting that loss of ANKRD22 caused a decrease in the mitochondrial Ca<sup>2+</sup> level in macrophages. Next, to explore the effect of NFAT on inflammation, we treated activated mouse macrophages with 100 ng/mL NFAT inhibitors. ELISA showed significantly reduced levels of TNF- $\alpha$  and

IL1 $\alpha$  in the culture supernatant (Figure 6F). Inhibition of NFAT also resulted in decreased TNF- $\alpha$  concentration in the supernatant of LPS-activated THP-1 and RAW264.7 macrophages (Figure 6G). Western blot showed that NFAT in macrophages was increased to varying degrees 24 hours after stimulation with different IFN- $\gamma$  or LPS concentrations (Figure 6H–I). Finally, to investigate the regulation of *ANKRD22* deletion on NFAT expression in macrophages, NFAT expression was detected in LPS-activated *Ankrd22*<sup>-/-</sup> mouse macrophages by Western blot. NFAT expression was lower than that in activated *Ankrd22*<sup>+/+</sup> mouse macrophages (Figure 6J). These results indicated that the loss of ANKRD22 inhibited macrophage activation and cytokine secretion mediated by mitochondrial Ca<sup>2+</sup> and cytoplasmic NFAT, which reduced the inflammatory response.

### Identification of a Lead Compound That Inhibits Activity of ANKRD22

The earlier-described findings suggested that suppression of ANKRD22 might target the Lgr5<sup>+</sup> EPCs to improve gastric mucosal repair and reduce the inflammation of the gastric epithelium. Therefore, we aimed to identify an inhibitory small-molecule lead compound that could target ANKRD22. Using ANKRD22 homology modeling with Molecular Operating Environment software, we virtually screened the Chemdiv database (2019 version) (<https://www.chemdiv.com>), containing 1,535,478 small molecules. The interaction fingerprint pattern map showed that most small-molecule compounds were predicted to interact with ANKRD22 at the E115/D123 sites. In addition, there was a class of small molecules showing a unique mode of action that could interact directly with the Cys133 side chain, which mainly interacts with L122/D132 (Figure 7A). To verify whether these residues were necessary for the function of ANKRD22, E115A/D123A and L122A/D132A mutants were constructed. Because the endogenous expression levels of ANKRD22 in SGC7901 cells were very low, these cells were used as negative controls. ANKRD22-overexpressing cells were constructed successfully by transient transfection and were used as positive controls (Figure 7B). Because ANKRD22 could increase the

**Figure 4. (See previous page). ANKRD22 deletion suppresses the noncanonical Wnt-Ca<sup>2+</sup> pathway.** (A) Effect of *Ankrd22* knockout on the Wnt pathway in mouse gastric epithelium after mucosal injury detected by Western blot. (B) Effect of ANKRD22 on the Wnt pathway in cultured cells detected by Western blot. (C) *Ankrd22* knockout reduced the intracellular Ca<sup>2+</sup> levels in mouse gastric epithelial cells detected by Fluo-4-based FCM. *Ankrd22*<sup>+/+</sup> and *Ankrd22*<sup>-/-</sup> mice were subjected to subsequent detection at 24 hours after intragastric administration of EtOH/HCl or saline solution (Ctrl) (n = 4). (D) ANKRD22 increased the intracellular Ca<sup>2+</sup> levels in gastric cancer cells. (E) Mitochondrial colocalization of the exogenous-expressing ANKRD22 in the organoid-enriched gastric cancer cells detected by confocal microscopy. (F and G) *Ankrd22* knockout reduced the mitochondrial Ca<sup>2+</sup> level in mouse gastric epithelium. *Ankrd22*<sup>+/+</sup> and *Ankrd22*<sup>-/-</sup> mice were subjected to subsequent detection at 24 hours after intragastric administration of EtOH/HCl (n = 3). Confocal microscopy was used to compare the fluorescence intensity and colocalization with mitochondria. The fluorescence intensity was detected by Rhod-2-based FCM. (H) Inhibition of the Wnt-Ca<sup>2+</sup> pathway increased the canonical Wnt pathway activity in the gastric cancer cells detected by Western blot. (I) Inhibition of the Wnt-Ca<sup>2+</sup> pathway increased the number of organoid-enriched primary mouse gastric EPCs. (H and I) The cells were cultured for 24 hours in medium with or without (Ctrl) 10  $\mu$ mol/L FK506 or KN93. (J–L) *Ankrd22* knockout decreased the levels of diacylglycerol (DAG) phosphorylated-CaMKII, and NFAT in the mouse gastric epithelium after mucosal injury detected by Western blot (n = 3). (M) Expression of NFAT1 in the *Ankrd22*<sup>+/+</sup> and *Ankrd22*<sup>-/-</sup> mouse gastric epithelium after mucosal injury detected by IHC staining. Normal mouse IgG was used as a negative control (Ctrl). *Ankrd22*<sup>+/+</sup> and *Ankrd22*<sup>-/-</sup> mice were subjected to subsequent detection at 24 hours after intragastric administration of EtOH/HCl. The data were analyzed by the Student *t* test and are presented as means  $\pm$  SD. \**P* < .05 and \*\**P* < .01. p-CaMKII, Phosphorylated calcium/calmodulin-dependent protein kinase type II.

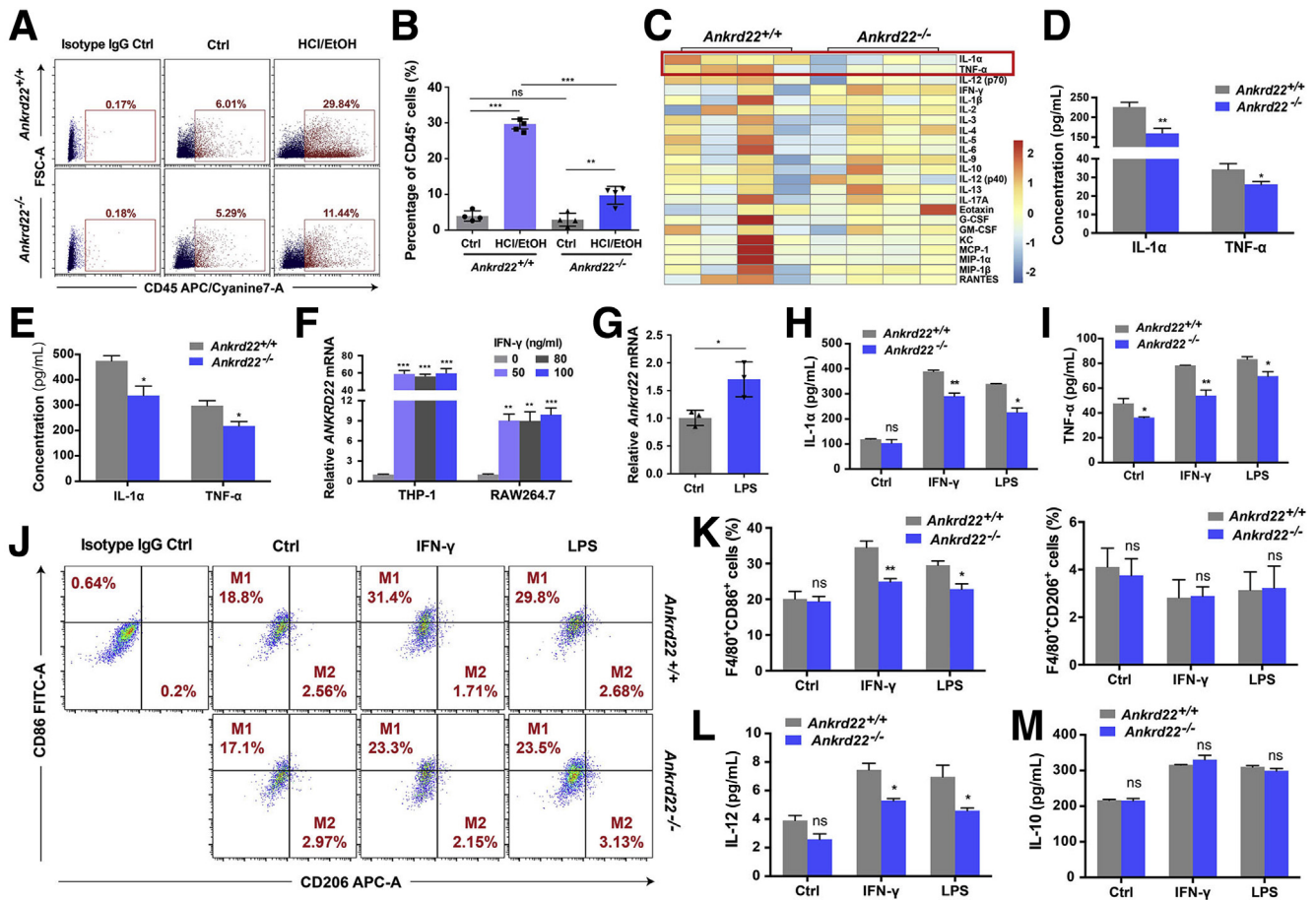


**Figure 5. ANKRD22 deletion reduces the inflammatory response by inhibiting activation of the macrophages after gastric mucosal injury.** (A and B) *Ankrd22* knockout decreased the number of CD45<sup>+</sup> cells in damaged mouse gastric mucosa detected by FCM. Rat IgG2b was used as an isotype control ( $n = 4$ ). (C and D) Effect of *Ankrd22* knockout on the expression profiles of inflammatory factors in damaged mouse gastric mucosa detected by Luminex assay ( $n = 4$ ). (E) *Ankrd22* knockout reduced IL1 $\alpha$  and TNF- $\alpha$  in mouse damaged gastric mucosa detected by ELISA ( $n = 3$ ). (A–E) *Ankrd22*<sup>+/+</sup> and *Ankrd22*<sup>-/-</sup> mice were examined 24 hours after intragastric administration of EtOH/HCl or saline solution (Ctrl). (F) Expression levels of ANKRD22 in the macrophages activated by different concentrations of IFN- $\gamma$ . THP-1 and RAW264.7 macrophages were stimulated with 0, 50, 80, or 100 ng/mL IFN- $\gamma$  for 24 hours. Subsequently, the expression of ANKRD22 was determined by qRT-PCR. The data from the 0 ng/mL group were normalized to 1.0. *TUBB* and *Tubb* were used as internal references. (G) Expression levels of *Ankrd22* in the activated mouse macrophages detected by qRT-PCR. Data of the PBS-treated group (Ctrl) were normalized to 1.0. *Tubb* was used as an internal reference. (H and I) Determination of IL1 $\alpha$  and TNF- $\alpha$  in supernatant of activated macrophages from *Ankrd22*<sup>+/+</sup> or *Ankrd22*<sup>-/-</sup> mice by ELISA. (J and K) Effects of *Ankrd22* knockout on the percentages of CD86<sup>+</sup> and CD206<sup>+</sup> cells in activated *Ankrd22*<sup>+/+</sup> and *Ankrd22*<sup>-/-</sup> mouse macrophages detected by FCM. Rat IgG2b was used as an isotype control ( $n = 3$ ). (L and M) Determination of IL12 (p70) and IL10 in the supernatant of activated macrophages from *Ankrd22*<sup>+/+</sup> or *Ankrd22*<sup>-/-</sup> mice by ELISA. (E–M) Macrophages were stimulated with 50 ng/mL IFN- $\gamma$  or 100 ng/mL LPS or PBS (Ctrl) for 24 hours. The data were analyzed by the Student *t* test and are presented as means  $\pm$  SD. \* $P < .05$ , \*\* $P < .01$ , and \*\*\* $P < .001$ . APC-A, Allophycocyanin Area; FITC-A, Fluorescein Isothiocyanate Area; FSC-A, Forward Scatter Area.

intracellular Ca<sup>2+</sup> concentration as its key mechanism for the repair of gastric mucosal damage, we evaluated the effects of the ANKRD22 mutants on the intracellular Ca<sup>2+</sup> concentrations. FCM analysis based on Fluo-4 was used to detect changes in the intracellular Ca<sup>2+</sup> levels. We found that the Ca<sup>2+</sup> levels did not change significantly between the SGC7901 cells expressing the E115A/D123A mutant and those expressing the WT ANKRD22 (Figure 7C). By contrast, the L122A/D132A mutant significantly reduced the levels of intracellular Ca<sup>2+</sup> in gastric cancer cells compared with those in WT ANKRD22 cells (Figure 7D), suggesting that a

small-molecule compound interacting with the L122/D132 sites would inhibit the activity of ANKRD22. Using the molecular docking model, we screened the compounds that interacted more tightly with the L122/D132 sites and identified the ANKRD22-inhibiting lead compound, AV023 (Figure 7E).

To verify the biological function of AV023, we treated the ANKRD22-expressing SGC7901 cells with 0.05–1.0  $\mu$ mol/L AV023 for 24 hours and measured the *LGR5* mRNA levels in the cells by qRT-PCR. A significant increase in the expression of *LGR5* was observed after treatment with

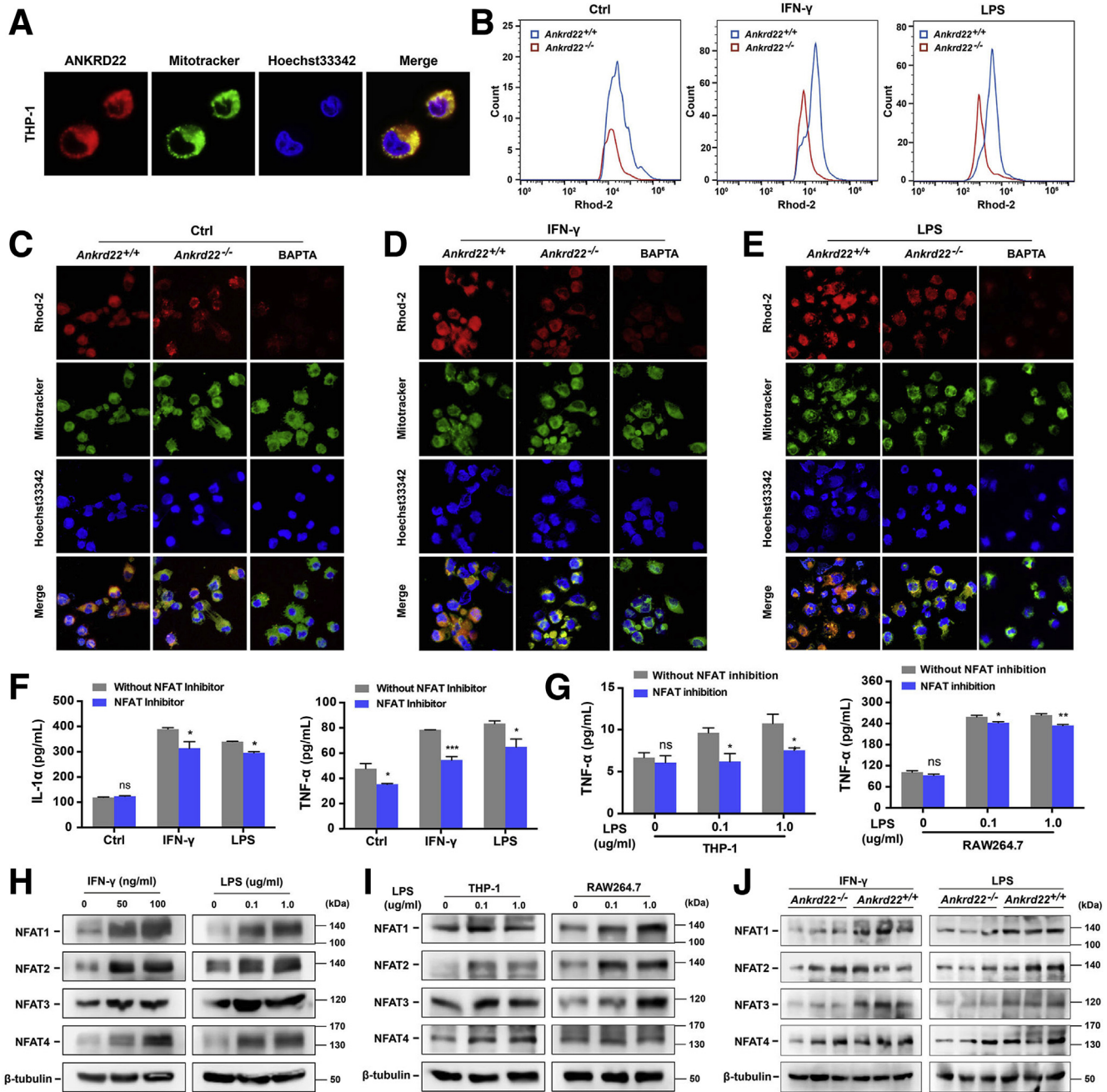
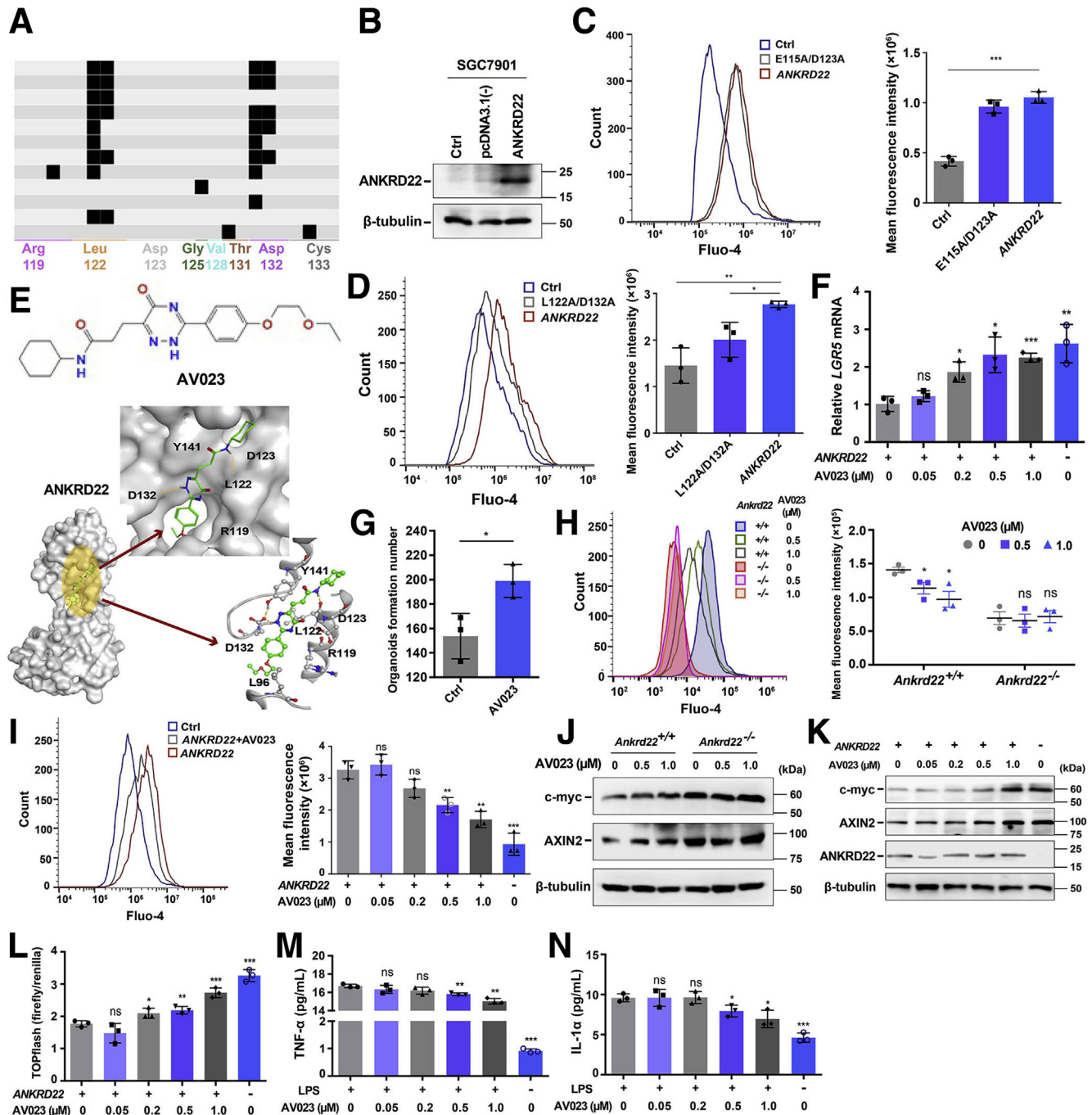


**Figure 6. ANKRD22 deletion reduces the expression levels of mitochondrial  $Ca^{2+}$  and cytoplasmic NFAT in macrophages.** (A) Mitochondrial colocalization of exogenous-expressing ANKRD22 in THP-1 macrophages detected by confocal microscopy. (B–E) *Ankrd22* knockout reduced the mitochondrial  $Ca^{2+}$  level in activated mouse macrophages. Confocal microscopy was used to compare the fluorescence intensity and colocalization with mitochondria. Macrophages treated with 50  $\mu$ mol/L 1,2-bis(o-aminophenoxy)ethane-N,N,N',N'-tetraacetic acid (BAPTA) for 24 hours was used as a negative control. The fluorescence intensity was detected by Rhod-2–based FCM. (F) Determination of IL1 $\alpha$  and TNF- $\alpha$  in supernatant of activated mouse macrophages by ELISA after NFAT inhibition. The activated macrophages were treated with 100 ng/mL NFAT inhibitor for 1 hour. (B–F) Macrophages were stimulated with 50 ng/mL IFN- $\gamma$  or 100 ng/mL LPS or PBS (Ctrl) for 24 hours. (G) Determination of TNF- $\alpha$  in the supernatant of activated macrophages by ELISA after NFAT inhibition. The LPS-activated macrophages were treated with 100 ng/mL NFAT inhibitor for 1 hour. (H) Detection of NFAT in the activated mouse macrophages by Western blot. (I) Detection of NFAT in the activated macrophages by Western blot. (G–I) THP-1 macrophages were treated with 100 ng/mL phorbol 12-myristate 13-acetate for 24 hours in advance. (J) Effects of *Ankrd22* knockout on the expression levels of NFAT in activated mouse macrophages detected by Western blot. Macrophages were stimulated with 50 ng/mL IFN- $\gamma$  or 100 ng/mL LPS for 24 hours. Macrophages were stimulated with 0, 50, or 100 ng/mL IFN- $\gamma$  or 0, 0.1, or 1.0  $\mu$ g/mL LPS for 24 hours. Data are presented as means  $\pm$  SD and analyzed using the Student *t* test. \**P* < .05 and \*\**P* < .01.

0.2–1.0  $\mu\text{mol/L}$  AV023 (Figure 7F). In addition, the number of clones derived from the organoid culture was significantly higher in the primary *Ankrd22*<sup>+/+</sup> mouse gastric EPCs that were treated with 1.0  $\mu\text{mol/L}$  AV023 than that in the untreated group (Figure 7G), suggesting that AV023 promoted the proliferation of gastric EPCs in vitro. Measurement of  $\text{Ca}^{2+}$  levels in the gastric epithelial cells of *Ankrd22*<sup>+/+</sup> mice using FCM based on Fluo-4 showed that the  $\text{Ca}^{2+}$  levels decreased after treatment with 0.5–1.0  $\mu\text{mol/L}$  AV023 (Figure 7H), consistent with the changing trend of  $\text{Ca}^{2+}$  levels in ANKRD22<sup>+</sup>

SGC7901 cells (Figure 7I). In addition, both Western blot and the TOPflash luciferase reporter assay (Promega, Madison, WI) showed that the activity of the Wnt pathway was up-regulated significantly in the gastric cells of *Ankrd22*<sup>+/+</sup> mice and ANKRD22<sup>+</sup> SGC7901 cells after AV023 treatment, but not in the gastric cells of *Ankrd22*<sup>-/-</sup> mice (Figure 7J–L), which also suggested that AV023 especially targets ANKRD22. Finally, to evaluate the effect of AV023 on inflammation, mouse macrophages activated with 100 ng/mL LPS were treated with 0.05–1.0  $\mu\text{mol/L}$  AV023 for 24 hours. ELISA showed a significant decrease



in the levels of TNF- $\alpha$  and IL1 $\alpha$  in the culture supernatant after treatment with 0.5–1.0  $\mu\text{mol/L}$  AV023 (Figure 7M and N). These results suggested that the inhibitory lead compound, AV023, showed effects similar to those caused by the deletion of ANKRD22 in vitro and could be used as a potential gastric mucosal protective agent targeting the progenitor cells and macrophages.

### Inhibitory Lead Compound Targeting ANKRD22 Alleviates Gastric Mucosal Injury In Vivo

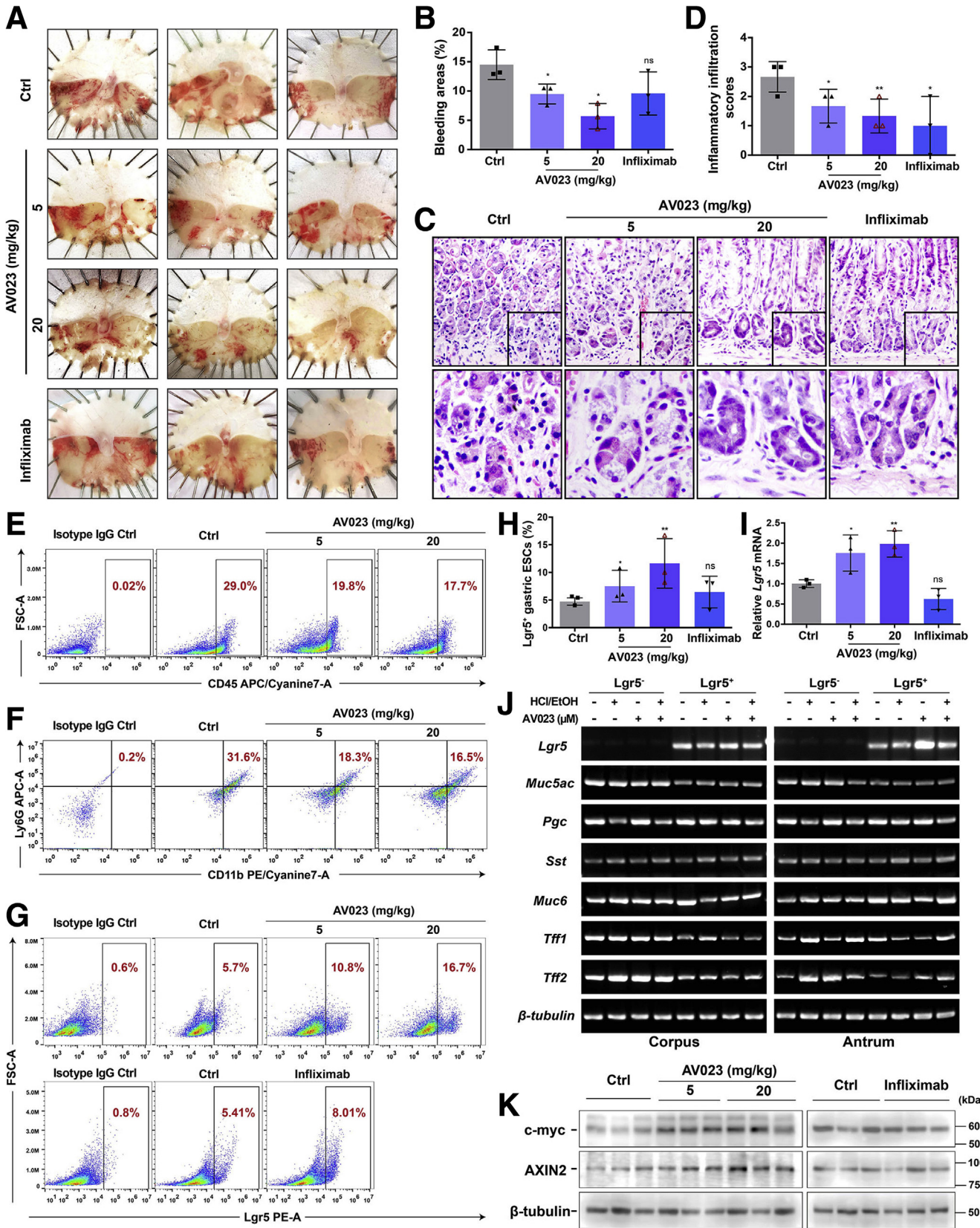
To assess whether AV023 reduces the effect of gastric mucosal damage similar to that observed in *Ankrd22* knockout mice in vivo, we explored the effects of AV023 on the accumulation of Lgr5<sup>+</sup> EPCs and the inflammatory response in a mouse model of acute gastric mucosal injury. Two groups of *Ankrd22*<sup>+/+</sup> mice were injected intraperitoneally with 5 or 20 mg/kg AV023 in vitro, which corresponded to the concentrations of 0.5 and 1.0  $\mu\text{mol/L}$ , respectively, 2 hours after EtOH/HCl-induced damage to the mouse gastric mucosa. Another group of mice was used as an inflammatory inhibition group and injected intraperitoneally with 10 mg/kg of infliximab, which targets TNF- $\alpha$ . The same amount of saline solution was administered to the control group. At 24 hours after injection, gastric mucosal damage, as indicated by the percentage of bleeding areas, was lessened significantly in the AV023-treated mice compared with the control mice, especially at a concentration of 20 mg/kg. Gastric damage was not reduced significantly in the anti-TNF- $\alpha$  agent group (Figure 8A and B). These findings suggested that AV023 alleviated the gastric mucosal damage. H&E staining further showed that inflammatory cell infiltration into the mouse gastric epithelium was reduced significantly after treatment with either AV023 or infliximab (Figure 8C and D). FCM showed that the percentages of CD45<sup>+</sup> leukocytes and CD11b<sup>+</sup>Ly6G<sup>+</sup> neutrophils were significantly lower in the gastric epithelium of the AV023-treated mice than in the control mice (Figure 8E and F), suggesting that AV023 had a suppressive effect on

local inflammation of injured gastric mucosa, particularly reducing the neutrophil infiltration. FCM and qRT-PCR analyses detected the proportion of Lgr5<sup>+</sup> EPCs and the *Lgr5* mRNA levels, respectively, in the mouse gastric epithelium after the aforementioned treatments. These parameters were increased significantly after treatment with AV023 in a dose-dependent manner compared with those after control treatment with normal saline. By contrast, these 2 parameters did not change significantly in the anti-TNF- $\alpha$  agent group (Figure 8G–I). Moreover, PCR showed that Lgr5<sup>+</sup> cells in corpus and antrum treated with AV023 also expressed different gastric epithelial markers of *Muc5ac*, *Pgc*, *Sst*, *Muc6*, *Tff1*, and *Tff2* (Figure 8J), suggesting that AV023 does not affect the differentiation potentials of the Lgr5<sup>+</sup> EPCs. Finally, c-Myc and AXIN2 levels in the gastric epithelium were detected by Western blot. Both levels were higher in the treated groups than in the control group (Figure 8K). Taken together, these results indicate that the ANKRD22-inhibiting lead compound, AV023, could facilitate the repair of gastric mucosal damage, while promoting the accumulation of the Lgr5<sup>+</sup> EPCs and reduction of local inflammation, and potentially up-regulating the activity of the Wnt pathway.

## Discussion

In this study, we explored the role of ANKRD22 in the repair of gastric mucosal damage. We found that loss of ANKRD22 activated the canonical Wnt pathway by reducing mitochondrial Ca<sup>2+</sup> levels and the cytoplasmic expression of NFAT in gastric epithelial cells, thereby promoting the proliferation of Lgr5<sup>+</sup> EPCs in gastric mucosal damage. *Ankrd22* knockout also attenuated the activation of macrophages, thereby reducing the inflammation of the gastric epithelium. The ANKRD22-inhibiting lead compound also showed similar effects, suggesting its potential therapeutic applications. The collective data suggest that the inhibition of ANKRD22 may be a potential therapeutic approach for the rapid repair of gastric mucosal damage.

**Figure 7. (See previous page). Identification of a lead compound that inhibits the activity of ANKRD22.** (A) Small molecules interacting with the L122/D132 sites of ANKRD22 predicted by protein ligand interface fingerprint software. (B) Expression levels of ANKRD22 in the WT, empty vector-transfected, or ANKRD22/pcDNA3.1(-)-transfected SGC7901 cells detected by Western blot. (C) Effect of the E115A/D123A mutant on intracellular Ca<sup>2+</sup> levels in ANKRD22<sup>+</sup> gastric cancer SGC7901 cells. The fluorescence intensity was detected using Fluo-4-based FCM. (D) Effect of the L122A/D132A mutant on the intracellular Ca<sup>2+</sup> levels in ANKRD22<sup>+</sup> gastric cancer SGC7901 cells. The fluorescence intensity was detected by Fluo-4-based FCM. (E) Schematic diagram of the chemical structure and acting sites of the ANKRD22 inhibitory lead compound-AV023. (F) Effects of AV023 on *LGR5* in ANKRD22<sup>+</sup> SGC7901 cells detected by qRT-PCR. SGC7901 cells without ANKRD22 overexpression were used as the control groups and the cells were treated with 0, 0.05, 0.2, 0.5, and 1.0  $\mu\text{mol/L}$  AV023 for 24 hours. *TUBB* was used as an internal reference. (G) AV023 increased the clone number of primary mouse gastric epithelial cells in organoid culture. *Ankrd22*<sup>+/+</sup> mouse gastric EPCs were treated with 0 (Ctrl) or 1.0  $\mu\text{mol/L}$  AV023 for 24 hours. (H) AV023 reduced the intracellular Ca<sup>2+</sup> levels in *Ankrd22*<sup>+/+</sup> mouse gastric epithelial cells. The fluorescence intensity was detected by Fluo-4-based FCM. (I) AV023 reduced the intracellular Ca<sup>2+</sup> levels in ANKRD22<sup>+</sup> SGC7901 cells. The fluorescence intensity was detected by Fluo-4-based FCM. (J) AV023 increased the Wnt pathway activity in *Ankrd22*<sup>+/+</sup> mouse gastric organoids detected by Western blot. (K) AV023 increased the Wnt pathway activity in ANKRD22<sup>+</sup> SGC7901 cells detected by Western blot. (L) AV023 increased the Wnt transcriptional activity of ANKRD22<sup>+</sup> SGC7901 cells detected by TOPflash luciferase reporter assay. (H–L) *Ankrd22*<sup>+/+</sup> and *Ankrd22*<sup>-/-</sup> mouse gastric cells were treated with 0, 0.5, and 1.0  $\mu\text{mol/L}$  AV023 for 24 hours. SGC7901 cells without ANKRD22 overexpression were used as the control groups and the cells were treated with 0, 0.05, 0.2, 0.5, and 1.0  $\mu\text{mol/L}$  AV023 for 24 hours. (M and N) Effect of AV023 on the release of IL1 $\alpha$  and TNF- $\alpha$  in the activated mouse macrophages detected by ELISA. Mouse macrophages were stimulated with 100 ng/mL LPS for 24 hours, and the control group was not treated with LPS. Cells were treated with 0, 0.05, 0.2, 0.5, and 1.0  $\mu\text{mol/L}$  AV023 for 24 hours. The data were analyzed by the Student *t* test and are presented as means  $\pm$  SD. \**P* < .05, \*\**P* < .01, and \*\*\**P* < .001.



Active Lgr5<sup>+</sup> gastric EPCs are responsible for the self-renewal of normal gastric epithelial cells and contribute to the repair of damaged gastric mucosa.<sup>20–22</sup> However, the molecular mechanism underlying the repair of gastric mucosal damage by EPCs has not yet been elucidated clearly.<sup>23</sup> ANKRD22 is a reprogramming-related protein present in the colorectal cancer-initiating cells and Lgr5<sup>+</sup> intestinal stem cells.<sup>17</sup> It was highly expressed in normal gastric epithelial cells but the expression was decreased significantly after gastric mucosal damage, suggesting that activation of the stress pathway might induce the degradation of ANKRD22 in the stomach.

Among multiple gastric stemness-related markers, Lgr5 is affected most significantly by *Ankrd22* knockout after gastric mucosal injury. Because our study used EtOH/HCl to chemically induce mild to moderate gastric mucosal injury in mice, the damage may not have been sufficient to recruit earlier gastric epithelial stem cells, except EPCs. Therefore, *Ankrd22* knockout only promoted the proliferation of Lgr5<sup>+</sup> EPCs in this study, but had no significant effect on other stem cell markers. Although the proportion of Mist1<sup>+</sup> cells also increased after the deletion of ANKRD22, the large dispersion was not statistically significant, which may be owing to individual differences between the animals. The decreased ANKRD22 levels were accompanied by the increased proliferation of Lgr5<sup>+</sup> gastric EPCs and repair of the damaged gastric mucosa. This might be a novel mechanism to protect the gastric mucosa under stress. Lgr5<sup>+</sup> cells show different responses to injuries in the gastric corpus and antrum, which also represent different cell populations in different regions.<sup>8,20–22</sup> Lgr5<sup>+</sup> gastric cell proliferation does not respond to ANKRD22 deletion when the gastric tissue is not subject to any stress-related injury. More importantly, *Ankrd22* knockout promoted the proliferation of Lgr5<sup>+</sup> cells in both the corpus and antrum regions in the injured gastric mucosal cells, suggesting that this promotion was not region-specific. However, this result is inconsistent with our previous findings that ANKRD22 is highly expressed in the colorectal cancer-initiating cells and Lgr5<sup>+</sup> intestinal stem cells, which suggest that the epithelia of the stomach and intestinal tissues may show different modes of stress regulation.

Proliferation of the Lgr5<sup>+</sup> gastric EPCs is controlled by the Wnt pathway,<sup>7,24,25</sup> which in turn is regulated by the Ca<sup>2+</sup> concentration in the mitochondria.<sup>26–29</sup> In the current

study, we found that loss of ANKRD22 resulted in reduced mitochondrial Ca<sup>2+</sup> levels in gastric epithelial cells and a decrease in the expression levels of the downstream targets of the Wnt-Ca<sup>2+</sup> pathway, suggesting that ANKRD22 deletion might inhibit the activity of the Wnt-Ca<sup>2+</sup> pathway by reducing the mitochondrial Ca<sup>2+</sup> concentration and indirectly enhancing the activity of the canonical Wnt pathway, thereby regulating the proliferation of the Lgr5<sup>+</sup> gastric EPCs.

Besides proliferation of the Lgr5<sup>+</sup> gastric EPCs, the associated inflammatory response also influences the repair of the gastric mucosal damage. The inflammatory response associated with gastric mucosal injury is characterized by the expression of various proinflammatory factors.<sup>30</sup> Among these factors, TNF- $\alpha$  secreted by macrophages drives the activation of the inflammatory cells, while IL1 $\alpha$  promotes the release of TNF- $\alpha$ , which enhances the spread of inflammation.<sup>31</sup> Loss of ANKRD22 reduced the levels of TNF- $\alpha$  and IL1 $\alpha$  in the macrophages and led to a significant reduction in inflammation in a gastric injury model. Production and activation of inflammatory cytokines also were mediated by intracellular Ca<sup>2+</sup>.<sup>32</sup> Ca<sup>2+</sup> stimulates the activation of macrophages triggered by NFAT, thereby enhancing the inflammatory response.<sup>33</sup> Therefore, ANKRD22 deletion reducing the expression levels of NFAT as well as the Ca<sup>2+</sup> levels in the activated macrophages further explains the mechanism by which the absence of ANKRD22 reduces inflammation in injured gastric mucosal cells. It generally is believed that changes in the microenvironment in the tissue induce macrophages to differentiate into M2 type, which can inhibit inflammatory responses and play a role in tissue repair.<sup>34–36</sup> However, we did not observe any M2 polarization caused by *Ankrd22* knockout in our experiments. Instead, we found that ANKRD22 deletion inhibited the M1 polarization of macrophages, which may be closely related to the repair of gastric epithelial inflammatory damage.

Currently, clinical protection of the gastric mucosa is limited to symptomatic treatment to inhibit the levels of gastric acid and pepsin and improve ischemia.<sup>15,16</sup> Gastric mucosal protective agents targeting progenitor cells that can truly repair mucosal damage have not yet emerged. Therefore, ANKRD22 may be an ideal target for the development of novel gastric mucosal repair agents owing to its effects in promoting the proliferation of EPCs and

**Figure 8. (See previous page). Inhibitory lead compound targeting ANKRD22 alleviates gastric mucosal injury in vivo.** (A) Treatment with AV023 alleviated the gastric mucosal injury in mice. (B) AV023 reduced the bleeding areas in injured mouse gastric mucosa shown by ImageJ software. (C and D) Treatment with AV023 reduced inflammatory cell infiltration in injured mouse gastric mucosa detected by H&E staining. (E) Treatment with AV023 decreased the number of CD45<sup>+</sup> cells in the damaged mouse gastric mucosa detected by FCM. (F) Treatment with AV023 decreased the number of CD11b<sup>+</sup>Ly6G<sup>+</sup> cells in the damaged mouse gastric mucosa detected by FCM. (G and H) AV023 increased the number of Lgr5<sup>+</sup> EPCs in the mouse injured gastric mucosa detected by FCM. (I–H) Rat IgG2b was used as an isotype control. (I) Effect of AV023 on *Lgr5* in the damaged mouse gastric mucosa detected by qRT-PCR. The data from the control (Ctrl) group were normalized to 1.0. *Tubb* was used as an internal reference. (J) *Muc5ac*, *Pgc*, *Sst*, *Muc6*, *Tff1*, and *Tff2* were expressed in Lgr5<sup>+</sup> cells after treatment with AV023 as detected by PCR. Lgr5<sup>+</sup> gastric epithelial cells were obtained by FACS. (K) Effect of AV023 on the Wnt pathway in injured mouse gastric mucosa detected by Western blot. (A–K) *Ankrd22*<sup>+/+</sup> mice were stimulated intragastrically by EtOH/HCl for 2 hours in advance, intraperitoneally injected with 5 or 20 mg/kg AV023, or 10 mg/kg infliximab or saline solution (Ctrl), and examined at 24 hours (n = 3). The data were analyzed by the Student *t* test and are presented as means  $\pm$  SD. \**P* < .05 and \*\**P* < .01. APC-A, Allophycocyanin Area; FSC-A, Forward Scatter Area; PE-A, Phycoerythrin Area.

reducing inflammation. Neutrophil infiltration represents the acute inflammatory response in ethanol-induced gastric mucosal injury.<sup>37</sup> Furthermore, we identified both in vivo and in vitro conditions in which AV023 promotes the proliferation of the Lgr5<sup>+</sup> gastric EPCs and exerts anti-inflammatory effects, particularly aiding in the reduction of neutrophilic infiltration. These effects are similar to those caused by ANKRD22 deletion in mice. These findings indicate that AV023 has potential application as a novel gastric mucosal repair agent. After treating mice with the TNF- $\alpha$  antagonist infliximab, we observed that the mouse gastric mucosal injury was not repaired significantly and the Lgr5<sup>+</sup> gastric EPCs did not show significant proliferation. These observations suggest that inhibiting the inflammatory response alone is not sufficient to protect the gastric mucosa, and the rapid proliferation of gastric EPCs also may be needed for the effective repair of gastric mucosal injury.

Our results were observed in a mouse model in which acute gastric injury was induced with the EtOH/HCl solution. However, the reparative effect of AV023 on the chronic inflammation of human gastric mucosa caused by various pathogenic factors needs to be elucidated further.

In summary, ANKRD22 could be an ideal therapeutic target for inhibition that promotes the repair of gastric mucosal damage. Suppression of ANKRD22 can rapidly accelerate the proliferation of Lgr5<sup>+</sup> gastric EPCs and reduce local inflammation in the gastric epithelium. Moreover, AV023, an ANKRD22-inhibiting lead compound, may have potential application as a gastric mucosal repair agent. Therefore, the findings of this study provide a novel strategy for the development of target-based drugs to aid in the rapid repair of gastric mucosal injury.

## Methods

### Mice

*Ankrd22*<sup>-/-</sup> C57BL/6 mice were constructed by Cyagen Biosciences (Guangzhou, Guangdong, China) using the clustered regularly interspaced short palindromic repeats/Cas9 technology as described previously.<sup>17</sup> The *Ankrd22* knockout verification primers used were as follows: 5'-GCTGCCCTAAAGTCTTTCCTTCC-3' (forward) and 5'-GGGAGT ATCGCCATTGAAGCTATCT-3' (reverse), producing a fragment size of 383 bp with an annealing temperature of 57°C. The *Lgr5-EGFP-IRES-creERT2* knockin mice were purchased from Shanghai Model Organisms (China). Female WT C57BL/6 mice weighing 20–25 g were acquired from the Laboratory Animal Resources of the Chinese Academy of Sciences (Shanghai, China). All the animals were reared and bred at the Zhejiang Chinese Medical University Laboratory Animal Research Center. They were maintained at 25°C  $\pm$  3°C, 30%–70% humidity, and alternating 12 hours of normal light and dark cycles. They were fed standard laboratory food and water. The animals were starved for 12 hours before experiments but were allowed ad libitum access to water during fasting. All animal experiments were conducted with approval of the Medical Animal Ethics Committee of the Second Affiliated Hospital of Zhejiang

University School of Medicine and Zhejiang Chinese Medical University. All animals were handled in compliance with the local regulations of the Zhejiang Provincial Government and the American Association for the Accreditation of Laboratory Animal Care guidelines.

### Human Materials

Injured human gastric epithelial mucosa and corresponding uninjured mucosa were obtained from 20 chronic gastritis patients (8 men, 12 women; age, 28–75 y) who underwent gastroscopy. Gastric tissues with *H pylori* infection were obtained from 8 patients (4 men, 4 women; age, 25–67 y), and those without *H pylori* infection were obtained from 8 patients (4 men, 4 women; age, 20–51 y) who underwent gastroscopy. Gastric cancer tissues and the corresponding adjacent noncancerous epithelial tissues ( $\geq$ 5 cm) were obtained from 10 patients (7 men, 3 women; age, 45–86 y) who underwent partial or total gastrectomy. All samples were from the Second Affiliated Hospital of Zhejiang University School of Medicine. This study was approved by the ethical committee of the Second Affiliated Hospital of Zhejiang University School of Medicine.

### Cells and Cell Culture

The gastric cancer cells SGC7901 and BGC823 and human THP-1 macrophages were purchased from the Cell Bank of the Shanghai Branch of the Chinese Academy of Sciences. Mouse RAW264.7 macrophages were kindly provided by Professor Hongxiang Sun (College of Animal Sciences, Zhejiang University). Cells were cultured in the following media (Corning, Corning, NY) supplemented with 10% fetal bovine serum (FBS) (Corning) and 100  $\mu$ g/mL gentamicin (Sangon Biotech, Shanghai, China) at 37°C in a humidified 5% CO<sub>2</sub> atmosphere. Then, SGC7901 and BGC823 cells and human THP-1 macrophages were cultured in RPMI 1640 medium. Meanwhile, the mouse RAW264.7 macrophages were cultured in Dulbecco's modified Eagle medium (DMEM).

### Preparation of the Anti-ANKRD22 Antibody

The pET42a (Novagen, Madison, WI) prokaryotic vector expressing the human full-length ANKRD22 was constructed as we described previously.<sup>38</sup> The plasmid was transformed into *Escherichia coli* BL21 DE3 to induce the expression of the recombinant protein. After purification and identification of the ANKRD22 recombinant protein, HuaBio (Hangzhou, Zhejiang, China) was commissioned to conduct subsequent animal immunization, cell fusion, and hybridoma cell screening. Four ANKRD22 monoclonal antibodies (clone numbers 1A8, 1B1, 2E4, and 1F3) were obtained after identification by Western blot. Finally, the 1A8 monoclonal antibody cross-reacting with the mouse ANKRD22 was used in this study.

### Western Blot

The cells were digested and incubated in an ice-cold radioimmunoprecipitation assay (RIPA) lysis buffer

containing the protease inhibitor cocktail for 30 minutes. Then, the loading buffer (3×) was added to the samples and they were boiled at 100°C for 5 minutes. Sodium dodecyl sulfate–polyacrylamide gel electrophoresis was performed and the proteins were transferred to nitrocellulose membranes (Sartorius Stedim, Gottingen, Germany). The membranes subsequently were blocked with 5% nonfat milk in Tris-buffered saline (TBS)–Tween-20 at room temperature for 1 hour and incubated with the primary antibody at 4°C overnight with gentle shaking. The following primary antibodies were used:  $\beta$ -tubulin (HuaBio), c-Myc (Cell Signaling Technology, Danvers, MA), AXIN2 (Cell Signaling Technology), NFAT1 (Proteintech, Wuhan, Hubei, China), NFAT2 (Cell Signaling Technology), NFAT3 (Abcam, Cambridge, UK), NFAT4 (GeneTex, Irvine, CA), diacylglycerol (LifeSpan Bio-Sciences, Seattle, WA), phospho-CaMKII (Thr286; Cell Signaling Technology), and CaMKII (GeneTex). Subsequently, the membranes were washed 5 times with TBS–Tween-20 and incubated with horseradish peroxidase–labeled secondary antibody (Jackson ImmunoResearch Laboratories, West Grove, PA) at room temperature for 1 hour with gentle shaking. After washing 5 times, the membranes were incubated in the enhanced chemiluminescence solution (Perkin Elmer, Akron, OH) for 1 minute and imaged on a C-DiGit Blot Scanner (LI-COR Biosciences, Lincoln, NE).

### IHC Staining

IHC staining was performed according to the standard protocol. Briefly, the section slides of gastric tissues were maintained at 60°C for 30 minutes and then deparaffinized in xylene and rehydrated with a graded series of alcohol solutions. An antigen retrieval process was performed in 10 mmol/L EDTA buffer at 95°C for 15 minutes. After cooling to room temperature, the tissue sections were blocked with 3% hydrogen peroxide for 10 minutes. After washing gently with TBS, each section was incubated with following primary antibodies: anti-ANKRD22 (1:150) at room temperature for 1 hour, anti-BrdU (1:200; HuaBio) at 4°C overnight, anti-Lgr5 (1:100; HuaBio) at 4°C overnight, or anti-NFAT1 (1:100; Proteintech) at 4°C overnight. Normal mouse IgG was used as a negative control. After washing 3 times with TBS, the slides were incubated with biotinylated secondary antibody at room temperature for 20 minutes. Then, the tissue sections were rinsed gently with TBS and counterstained with hematoxylin. The diaminobenzidine substrate was added to the tissue sections and incubated for 5 minutes. The slides were sealed and finally observed by optical microscopy.

### Construction, Production, and Infection of the Recombinant Lentivirus

The construction and production of the ANKRD22 overexpression recombinant lentivirus was performed by Cyagen Biosciences. Cell infection with the recombinant lentivirus was performed in accordance with the company's operating instructions. To establish the ANKRD22 overexpression cells, 8  $\mu$ g/mL polybrene and an appropriate amount of virus were

added to the cells. The control cells were infected simultaneously with the corresponding blank vector lentivirus. After incubating for 48 hours, the cells were selected by treating with 5  $\mu$ g/mL puromycin for 2 weeks and the efficiency of infection was verified by Western blot.

### Immunofluorescence Colocalization Analysis

The gastric cancer cells SGC7901 and BGC823 were infected with a lentivirus expressing the Halo-ANKRD22 (Promega, Madison, WI) fusion protein. The cells were transferred to a 24-well plate preloaded with cover glasses (Nest, Wuxi, Jiangsu, China). On the following day, the cells were washed with phosphate-buffered saline (PBS) and incubated with 5  $\mu$ mol/L HaloTag Tetramethylrhodamine ligand at 37°C for 30 minutes in the dark. Subsequently, the cells were washed 3 times and incubated with 150 nmol/L MitoTracker Green FM (Invitrogen, Carlsbad, CA) at 37°C for 30 minutes in the dark. The cells then were washed 3 times and incubated with 5  $\mu$ g/mL Hoechst33342 dye at 37°C for 15 minutes in the dark. After the final washing, the cover glasses were taken out, sealed, and observed by confocal microscopy (Carl Zeiss, Jena, Germany). To detect the mitochondrial localization of ANKRD22 in the organoid-cultured gastric EPCs, SGC7901 and BGC823 cells overexpressing Halo-ANKRD22 fusion protein were cultured in the Matrigel (Corning, NY) matrix for 7 days. After recovery, the cells were placed onto the slides and treated as described earlier.

### EtOH/HCl-Induced Mouse Model of Acute Gastric Mucosal Injury

Acute gastric mucosal damage was induced in mice using the traditional method described in previous studies, with slight modifications.<sup>39</sup> After fasting for 12 hours, the animals were administered a solution of 60% EtOH in 150 mmol/L HCl (10 mL/kg weight) by gavage to induce gastric mucosal injury. To attain different degrees of gastric mucosal injury, the animals were administered different concentrations of acidified ethanol solutions (mild injury, 50% EtOH/150 mmol/L HCl; moderate injury, 70% EtOH/150 mmol/L HCl; severe injury, 90% EtOH/150 mmol/L HCl; all at 10 mL/kg weight).<sup>40</sup> The same amount of saline solution was administered to the control group. After treatment with EtOH/HCl and a 2-hour observation, the animals were euthanized by CO<sub>2</sub> inhalation at 0, 24, 48, or 72 hours. To inhibit the activity of ANKRD22 in vivo, the mice were stimulated intragastrically by EtOH/HCl for 2 hours, then injected intraperitoneally with 5 or 20 mg/kg AV023 or 10 mg/kg infliximab, and then killed 24 hours after the injection. The stomach of each mouse then was removed by cutting the tissue from the esophagus to the duodenum along the greater curve. The gastric tissue samples were rinsed with ice-cold saline solution to remove the gastric contents and blood clots. They were either used fresh or frozen in liquid nitrogen and stored at –80°C for subsequent experiments.

### *Histologic Examination and Assessment of the Degree of Inflammation*

H&E staining was performed according to the standard protocol. The stomach of each mouse was removed and fixed in 10% formalin for more than 48 hours. After dehydration in graded alcohol and embedding in paraffin wax, the thin sections were stained with H&E for histologic evaluation by optical microscopy. The scoring method of the degree of inflammation was modified from that reported previously by the same pathologist.<sup>41,42</sup> All assessments were performed blindly. The inflammatory damage score was classified as follows: 0, no inflammatory cell infiltration; 1, small amount of inflammatory cell infiltration in the lamina propria or epithelium or 1–2 infiltration foci; 2, moderate inflammatory cell infiltration or 3–4 infiltration foci; and 3, a large amount of inflammatory cell infiltration or more than 4 infiltration foci.

### *Dissociation of the Gastric Epithelial Cells*

Fresh gastric tissues from mice were cut into small pieces, placed in the serum-free RPMI 1640 medium containing 1 mg/mL type IV collagenase (Worthington, Lakewood, NJ) and 0.5 mg/mL hyaluronidase (Sigma-Aldrich, St. Louis, MO), and digested at 37°C for 90 minutes. The cells were separated by repeatedly aspirating and pipetting the chopped gastric tissues in the mixture. The mixture containing the separated epithelial cells then was filtered through a 70- $\mu$ m filter and centrifuged at  $720 \times g$  at 4°C for 5 minutes. The cell pellet was washed 3 times with ice-cold, serum-free RPMI 1640 medium for subsequent analysis.

### *FCM and FACS*

The primary gastric cells or macrophages ( $1 \times 10^7$ ) were digested into single cells and washed twice. The cell precipitates were blocked with buffer containing 2% FBS for 15 minutes. After centrifugation, the cells were incubated in buffer containing primary antibodies on ice for 30 minutes in the dark. The following primary antibodies were used: anti-mouse Lgr5-Phycoerythrin (PE, Miltenyi, Bergisch Gladbach, Germany), anti-human Lgr5-PE (BioLegend, San Diego, CA), Mist1 (Invitrogen), anti-mouse Sox2-Pacific Blue (BioLegend), Sox9 (HuaBio, China), anti-mouse CD44-fluorescein isothiocyanate (FITC) (BioLegend), anti-mouse CD133-PE/cyanine 7 (BioLegend), anti-mouse CD166-Allophycocyanin (APC, Miltenyi), anti-mouse SSEA1-FITC (BioLegend), anti-mouse SSEA4-Alexa Fluor 647 conjugated (R&D Systems, Minneapolis, MN), anti-mouse CD45-APC/cyanine 7 (BioLegend), anti-mouse F4/80-PE (Miltenyi), anti-mouse CD86-FITC (BioLegend), anti-mouse CD206-APC (BioLegend), anti-mouse CD11b-PE/cyanine 7 (BioLegend), and anti-mouse Ly6G-APC (BioLegend). APC goat anti-mouse IgG (BioLegend) was used as the secondary antibody and rat IgG2b (Miltenyi) was used as an isotype control. After washing with PBS, the cells were filtered and resuspended with 500  $\mu$ L buffer. The percentage of positive cells was detected by FACSCanto II flow cytometry (BD Biosciences, Franklin Lakes, NJ). The Lgr5<sup>+</sup> and Lgr5<sup>-</sup> mouse gastric epithelial cells were obtained using

a FACSria III flow sorter (BD Biosciences). FCM and FACS data were analyzed by FlowJo v.10.0 (Ashland, OR) or CytExpert 2.0 (Indianapolis, IN) software. When detecting the expression levels of Lgr5 and Ki67 in the organoid-cultured gastric EPCs, the mouse primary gastric cells were cultured in the Matrigel matrix for 7 days. After recovery and staining with the anti-mouse Lgr5-PE antibody (Miltenyi), the cells were fixed and the nuclear membrane was broken. Then, the cells were stained with the anti-mouse Ki67-FITC antibody (Miltenyi) and treated as described earlier.

### *Organoid Culture*

As described previously,<sup>24,43</sup> the primary gastric epithelial cells from mice were isolated and counted. Then, 500 cells/well were resuspended in 0.1 mL of serum-free DMEM, mixed with 0.1 mL growth factor-reduced Matrigel matrix (Corning), and seeded in 24-well ultra-low-attachment plates (Corning). After incubation at 37°C for 1 hour, 0.2 mL serum-free medium (DMEM/F12 medium supplemented with  $1 \times$  B27,  $1 \times$  N2, 5 mmol/L *N*-acetyl cysteine, 50  $\mu$ g/L epidermal growth factor, 100  $\mu$ g/L basic fibroblast growth factor, 100  $\mu$ g/L noggin, 10 mmol/L gastrin, 500  $\mu$ g/L R-spondin, 100 ng/mL Wnt3a, and 100  $\mu$ g/mL gentamicin) was added. To inhibit the activity of the Wnt-Ca<sup>2+</sup> pathway, the serum-free medium was supplemented with 10  $\mu$ mol/L of the NFAT inhibitor FK506 or the CaMKII inhibitor KN93 (Selleck Chemicals, Houston, TX). Then, the cells were cultured at 37°C in a humidified 5% CO<sub>2</sub> atmosphere.

After 5–7 days, organoid clones with a diameter greater than 50  $\mu$ m were counted under a microscope (Olympus, Tokyo, Japan). For the recovery of cells from organoids, the supernatants were removed and replaced with a cell recovery solution (Corning) mixed with the collected Matrigel matrix at a ratio of 1:1. After gentle shaking at 4°C for 2 hours, the mixture was centrifuged at  $1000 \times g$  at 4°C for 10 minutes and the cell pellet was harvested for subsequent FCM or immunofluorescence colocalization analysis.

### *RNA Extraction, RT-PCR, and qRT-PCR*

Total RNA was extracted from cells using the TRIzol reagent (Macherey-Nagel, Dueren, Germany). According to the manufacturer's instructions, the extracted RNA was reverse-transcribed to complementary DNA using a PrimeScript RT Reagent Kit (TaKaRa Bio, Kyoto, Japan). Subsequently, the PCR amplification was performed with the PrimeSTARHS DNA polymerase kit (TaKaRa Bio) at 98°C for 10 seconds, followed by 30 cycles of PCR at 60°C for 15 seconds, and 72°C for 1 min/kb using the Life Express TC-96 system (Bioer, Hangzhou, Zhejiang, China). Then, qRT-PCR was conducted using the Premix Ex Taq Kit (TaKaRa Bio) at 95°C for 30 seconds, followed by 40 cycles of 95°C for 5 seconds, and 60°C for 30 seconds in the CFX Connect system (Bio-Rad, Hercules, CA). The primers and probes were chemically synthesized by Sangon Biotech and are listed in Tables 1 and 2.

**Table 1.** Primers Used in PCR

Gene name	Sequence	Strand
<i>Lgr5</i>	5'-GCAGTGCTCGCCTTCCCAG-3'	Forward
	5'-CCGTCTTCCCACGCACC-3'	Reverse
<i>Muc5ac</i>	5'-GACCGTGTGGTGCTGACCCG-3'	Forward
	5'-GCCCTTGGCAGGAAGGCTGG-3'	Reverse
<i>Pgc</i>	5'-CAGAGCGAGGCCTGCACCAC-3'	Forward
	5'-AGAGGGGCTGGGACAGAGCG-3'	Reverse
<i>Sst</i>	5'-CTGGCTGCGCTCTGCATCGT-3'	Forward
	5'-AGCTTTGCGTTCCTGGGGTG-3'	Reverse
<i>Muc6</i>	5'-TGAGCTGTCCACGGCAAGCG-3'	Forward
	5'-CACACTGCCCCTCGCTGT-3'	Reverse
<i>Tff1</i>	5'-CGCTGTGGTCTCATGCTGGC-3'	Forward
	5'-GCCATGGGGTGAAGCACCA-3'	Reverse
<i>Tff2</i>	5'-TCCCCTGTCCGTGCTCCAG-3'	Forward
	5'-CGACTGGCACAGTCTCGGG-3'	Reverse
<i>Tubb</i>	5'-TGCCAAGGCTGTGGGCAAGG-3'	Forward
	5'-CAGCCCGGCATCGAAGGTG-3'	Reverse

### Determination of the Intracellular Ca<sup>2+</sup> Levels

A total of  $1 \times 10^6$  gastric cancer cells or primary gastric epithelial cells from mice were digested into single cells as described earlier and incubated in a buffer containing 10  $\mu\text{mol/L}$  Fluo-4 calcium indicator (Invitrogen) and 0.02% Pluronic F-127 (Sigma-Aldrich) at 37°C for 1 hour in the dark. Fluorescence then was measured on a FACSCanto II flow cytometer (BD, San Jose, CA). FCM data were analyzed by FlowJo v.10.0 software. The mean fluorescence intensity represented the intracellular Ca<sup>2+</sup> levels.

### Detection of Mitochondrial Ca<sup>2+</sup> Levels

The mitochondrial Ca<sup>2+</sup> levels in the macrophages were traced by Rhod-2 (Genmed, Shanghai, China) for fluorescence colocalization or FCM detection. For fluorescence colocalization detection, the frozen sections of mouse stomach tissues or macrophages on cover glasses (Nest) were washed twice and incubated with 10  $\mu\text{mol/L}$  Rhod-2 at 37°C for 1 hour in the dark. Subsequently, the cells were washed 3 times and stained with 150 nmol/L Mito-Tracker Green FM (Invitrogen) at 37°C for 30 minutes in the dark. Then, the cells were washed 3 times and incubated with 5  $\mu\text{g/mL}$  Hoechst33342 dye at 37°C for 15 minutes in the dark. After the final wash, the cover glasses were taken out, sealed, and observed by confocal microscopy (Carl Zeiss). For FCM detection, after digestion into single cells, the mouse gastric epithelial cells or macrophages were incubated in buffer containing 10  $\mu\text{mol/L}$  Rhod-2 fluorescent dye at 37°C for 1 hour in the dark. Fluorescence intensity then was detected by FACSCanto II flow cytometry (BD). The mean fluorescence intensity represented the mitochondrial Ca<sup>2+</sup> level.

### Luminex Assay

The stomach tissues of *Ankrd22*<sup>+/+</sup> and *Ankrd22*<sup>-/-</sup> mice were ground and homogenized with a corresponding volume of the RIPA lysis buffer (50 mmol/L Tris-HCl buffer, pH

7.4, 150 mmol/L NaCl, 1 mmol/L EDTA, 1% Triton X-100, 0.25% deoxycholate,  $1 \times$  protease inhibitor cocktail; Calbiochem, Darmstadt, Germany). The tissue lysate protein samples were prepared by centrifugation and sonication. According to the standard protocol of the Luminex Array Detection Kit (Bio-Plex Pro Mouse Cytokine Grp I Panel 23-plex; Bio-Rad), 23 mouse inflammatory factors were detected. The beads and samples were added to a 96-well plate and incubated for 30 minutes at room temperature in the dark. After washing 3 times, the samples were incubated with 25  $\mu\text{L}$  detection antibody per well at room temperature for 2 hours in the dark. After washing 3 times, 50  $\mu\text{L}$  streptavidin-phycoerythrin was added to each well and the samples were incubated at room temperature for 10 minutes. After final washing, the signal was detected using the Bio-Plex MAGPIX System (Bio-Rad).

### Determination of IL1 $\alpha$ , TNF- $\alpha$ , IL12, and IL10 Levels

Gastric tissue samples were ground and homogenized with ice-cold RIPA lysis buffer containing the protease inhibitor cocktail. The culture supernatant of the macrophages was collected and frozen at -20°C until measurement. According to the manufacturer's instructions, the cytokine levels of IL1 $\alpha$ , TNF- $\alpha$ , IL12, and IL10 in the samples were determined using ELISA kits (Proteintech). Ninety-six-well plates were coated with the antibodies to IL1 $\alpha$ , TNF- $\alpha$ , IL12, and IL10 at 4°C overnight. After blocking with buffer containing 2% FBS for 1 hour, the samples and standards were added at various dilutions and incubated at 37°C for 1 hour. After washing 3 times, the samples were incubated with the biotinylated detection antibody (diluted 1:1000) with buffer containing 1% bovine serum albumin at 37°C for 1 hour. After washing 3 times, the samples were incubated with horseradish peroxidase-labeled streptavidin antibody (diluted 1:5000) at 37°C for 1 hour. After the final washing, 100  $\mu\text{L}$  3, 3', 5, 5'-tetramethylbenzidine chromogenic substrate was added and reacted at 37°C for 20 minutes. Subsequently, 50  $\mu\text{L}$  stop solution was added to each well and the absorbance (optical density) was measured at 450 nm using a microplate reader.

### Separation and Treatment of Mouse Peritoneal Macrophages

Mice were stimulated with 1 mL 3% thioglycolate broth (Sigma-Aldrich) for 4 days in advance by intra-peritoneal injection. After death, each mouse was injected with 5 mL serum-free RPMI 1640 medium in the abdominal cavity. The abdominal fluid was lavaged out and centrifuged. The cell precipitate was washed with PBS before plating. After activation by 0, 50, or 100 ng/mL INF- $\gamma$  (Novoprotein, Shanghai, China) or 0, 0.1, or 1.0  $\mu\text{g/mL}$  LPS from *E coli* O55:B5 (Sigma-Aldrich) for 24 hours, the macrophages were treated with 50  $\mu\text{mol/L}$  1,2-bis(o-aminophenoxy)ethane-N,N,N',N'-tetraacetic acid (Selleck) for 24 hours or with 100 ng/mL NFAT inhibitor (Adooq, Irvine, CA) for 1 hour. The control group was not

**Table 2.** Primers and Probes Used in qRT-PCR

Gene name	Sequence	Strand	Modification
<i>ANKRD22</i>	5'-CCAGCTTGGACTTCTAGGGA-3' 5'-GGCAGATGGGCTCAGAGTAT-3' 5'-TCCCATGCTGGTCCCTTCACAGG-3'	Forward Reverse Probe	5'Fam-3'Tamra
<i>LGR5</i>	5'-AGCAAACCTACGTCTGGACA -3' 5'-ATGCTGGAGCTGGTAAAGGT-3' 5'-TCCTGTGACTCAACTCAAGCCTTGGT-3'	Forward Reverse Probe	5'Fam-3'Tamra
<i>TUBB</i>	5'-AGGAGGTCGATGAGCAGATG-3' 5'-TTGCCAATGAAGGTGACTGC-3' 5'-TGTGACATCCCACCTCGTGGCC-3'	Forward Reverse Probe	5'Fam-3'Tamra
<i>Ankrd22</i>	5'-CCAAGGCCTTCATCTCTCCA-3' 5'-GGCCAAGTCTTCAGAGGGAT-3' 5'-AGGACCCATTGCTCACGTTGGAATCT-3'	Forward Reverse Probe	5'Fam-3'Tamra
<i>Lgr5</i>	5'-TGGGCAAAGTAGGATTCGGT-3' 5'-CATCGAACACCTGCGTGAAT-3' 5'-AGCTGTGTCTTGTTCGGATCAACCA-3'	Forward Reverse Probe	5'Fam-3'Tamra
<i>Mist1</i>	5'-GCAGGACCTACATGTCCCTT-3' 5'-TCCTGCTATCCCAGACTCCT-3' 5'-AGGATCTTAGAGACTCCGGTCCCGT-3'	Forward Reverse Probe	5'Fam-3'Tamra
<i>Sox2</i>	5'-TGATGGAGACGGAGCTGAAG-3' 5'-TTCTCCTGGGCCATCTTACG-3' 5'-CGCCGTGGCGTTGCCTCCTC-3'	Forward Reverse Probe	5'Fam-3'Tamra
<i>Sox9</i>	5'-TTCAGATGCAGTGAGGAGCA-3' 5'-CTTGCAGAGGCATGTGTTGT-3' 5'-CCCGTGTCAACACACGCACA-3'	Forward Reverse Probe	5'Fam-3'Tamra
<i>Cd44</i>	5'-GGCACTGGCTCTGATTCTTG-3' 5'-CACCGTTGATCACCAGCTTT-3' 5'-CCTACTATTGACCGCGATGCAGACGG-3'	Forward Reverse Probe	5'Fam-3'Tamra
<i>Cd133</i>	5'-TGTC AACCTAGAGCAGGCAA-3' 5'-TAAACCGCAGGTAGCTCCAA-3' 5'-TGCCCTTCCTTGTGGATTCTGTCTGC-3'	Forward Reverse Probe	5'Fam-3'Tamra
<i>Cd166</i>	5'-AGAAACCGCGCTACCTTGA-3' 5'-CACACCCTTCCTCAGTGTCT-3' 5'-ACTCCCAGGACGGCGACCC-3'	Forward Reverse Probe	5'Fam-3'Tamra
<i>Ssea1</i>	5'-CCTCTTCTGTGACTCGTGA-3' 5'-ATCCCTGCAAAGTAGGCAGT-3' 5'-TGCCCAAGTAAACACAAGGCGGCA-3'	Forward Reverse Probe	5'Fam-3'Tamra
<i>Ssea4</i>	5'-GGGCGTATAGCAGAACCCTCT-3' 5'-CCCCTTCTCATCACAGCAG-3' 5'-CAGGGCTCGAACCATCGCACA-3'	Forward Reverse Probe	5'Fam-3'Tamra
<i>Tubb</i>	5'-ACCTTGCCTTACCTCTGACC-3' 5'-CACAAAGGGCAGGAACATACG-3' 5'-ACCCACTCCTGACCCAGCACC-3'	Forward Reverse Probe	5'Fam-3'Tamra

5'Fam, 5(6)-Carboxyfluorescein; 3'Tamra, 5(6)-Carboxytetramethylrhodamine.

treated with IFN- $\gamma$  or LPS. Human THP-1 cells were treated with 100 ng/mL phorbol 12-myristate 13-acetate (Sigma-Aldrich) for 24 hours in advance. The culture supernatant of the macrophages was collected and frozen at -20°C for subsequent experiments.

### Isolation of Mitochondria and the Residual Cytoplasmic Fraction

Mitochondria and the residual cytoplasmic fraction of cells and tissues were separated using the mitochondrial separation kit (Beyotime, Shanghai, China). ANKRD22-overexpressing cells and WT C57BL/6 mouse gastric tissues were washed with PBS twice, and an appropriate

amount of mitochondrial isolation reagent containing protease inhibitors was added. The cells were kept on ice for 15 minutes, homogenized 30 times, and centrifuged at 600  $\times g$  at 4°C for 10 minutes. The supernatant was centrifuged at 11,000  $\times g$  at 4°C for 10 minutes, and centrifuged again at 12,000  $\times g$  at 4°C for 10 minutes. The supernatant was saved as the residual cytoplasmic fraction and 100  $\mu$ L mitochondrial lysate containing protease inhibitors was added to the precipitate to obtain the mitochondrial fraction.

### ANKRD22 and the Construction of Mutants

The ANKRD22/pCMV5-XL5 plasmid (SC123169; OriGene, Rockville, MD) was subcloned into pcDNA3.1 (-)

(Invitrogen). Site-directed mutagenesis was performed on the *ANKRD22*/pcDNA3.1(-) plasmid at E115/D123 and L122/D132 sites using the MutanBEST Kit (TaKaRa Bio), according to the manufacturer's instructions. The E115A/D123A and L122A/D132A plasmids obtained after mutation then were used for cell transfection and subsequent experiments.

### TOPflash Luciferase Reporter Assay

The TOPflash luciferase reporter assay was performed using the luciferase reporter assay system (Promega), according to the manufacturer's instructions. *ANKRD22*<sup>+</sup> SGC7901 gastric cancer cells were transferred to a 6-well plate. TOP plasmid (Millipore, Darmstadt, Germany) and pRL plasmid (Promega) were transfected into the cells at a ratio of 4:1 with the Lipofectamine 3000 reagent (Invitrogen). The cells then were treated with different concentrations of AV023 for 24 hours. On the following day, after washing with PBS, the cells were incubated in 500  $\mu$ L 1 $\times$  passive lysis buffer at room temperature for 15 minutes with shaking. Subsequently, the cell lysate was transferred to a centrifuge tube. During the test, 20  $\mu$ L of the earlier-described cell lysate and 100  $\mu$ L LARII were added to the tube. After mixing, the luciferase activity was detected using the GloMax 20/20 Luminometer (Promega). Finally, 100  $\mu$ L Stop&Glo (Promega, Madison, WI) reagent was added to the tube to detect the Renilla luciferase activity.

### Assessment of Gastric Bleeding Areas

The fresh gastric tissues from mice were cut open in a longitudinal direction along the greater curvature, washed with precooled saline solution, and pinned flat on a cork board with the mucosal side up. The gastric tissues were photographed and the total stomach area as well as the bleeding areas were determined using ImageJ software (available from: <https://imagej.nih.gov/in>; National Institutes of Health, Bethesda, MD). The extent of gastric damage was quantified by calculating the percentage of bleeding areas. Based on this value, the efficiency of the repair of gastric injury by AV023 or infliximab was indicated.

### Statistical Analysis

All results for continuous variables are presented as means  $\pm$  SD. An unpaired 2-tailed Student *t* test was used for comparisons between 2 independent samples. Data were analyzed using SPSS v.23.0 statistical software (IBM, Armonk, NY). *P* < .05 was considered statistically significant. Statistical plots were constructed using GraphPad Prism v.7.0 software (San Diego, CA).

## References

- Mera RM, Bravo LE, Camargo MC, Bravo JC, Delgado AG, Romero-Gallo J, Yopez MC, Realpe JL, Schneider BG, Morgan DR, Peek RM Jr, Correa P, Wilson KT, Piazuelo MB. Dynamics of *Helicobacter pylori* infection as a determinant of progression of gastric precancerous lesions: 16-year follow-up of an eradication trial. *Gut* 2018;67:1239–1246.
- Lee YC, Chiang TH, Chou CK, Tu YK, Liao WC, Wu MS, Graham DY. Association between *Helicobacter pylori* eradication and gastric cancer incidence: a systematic review and meta-analysis. *Gastroenterology* 2016;150:1113–1124 e1115.
- Wallace JL. Prostaglandins, NSAIDs, and gastric mucosal protection: why doesn't the stomach digest itself? *Physiol Rev* 2008;88:1547–1565.
- Holt KM, Hollander D. Acute gastric mucosal injury: pathogenesis and therapy. *Annu Rev Med* 1986;37:107–124.
- Mills JC, Shivdasani RA. Gastric epithelial stem cells. *Gastroenterology* 2011;140:412–424.
- Wang C, Guo X, Xi R. EGFR and Notch signaling respectively regulate proliferative activity and multiple cell lineage differentiation of *Drosophila* gastric stem cells. *Cell Res* 2014;24:610–627.
- Barker N, Huch M, Kujala P, van de Wetering M, Snippert HJ, van Es JH, Sato T, Stange DE, Begthel H, van den Born M, Danenberg E, van den Brink S, Korving J, Abo A, Peters PJ, Wright N, Poulsom R, Clevers H. Lgr5(+ve) stem cells drive self-renewal in the stomach and build long-lived gastric units in vitro. *Cell Stem Cell* 2010;6:25–36.
- Leushacke M, Tan SH, Wong A, Swathi Y, Hajamohideen A, Tan LT, Goh J, Wong E, Denil S, Murakami K, Barker N. Lgr5-expressing chief cells drive epithelial regeneration and cancer in the oxyntic stomach. *Nat Cell Biol* 2017;19:774–786.
- Sigal M, Rothenberg ME, Logan CY, Lee JY, Honaker RW, Cooper RL, Passarelli B, Camorlinga M, Bouley DM, Alvarez G, Nusse R, Torres J, Amieva MR. *Helicobacter pylori* activates and expands Lgr5(+) stem cells through direct colonization of the gastric glands. *Gastroenterology* 2015;148:1392–1404 e1321.
- Ivashkiv LB. IFN $\gamma$ : signalling, epigenetics and roles in immunity, metabolism, disease and cancer immunotherapy. *Nat Rev Immunol* 2018;18:545–558.
- Huch M, Bonfanti P, Boj SF, Sato T, Loomans CJ, van de Wetering M, Sojoodi M, Li VS, Schuijers J, Gracanin A, Ringnalda F, Begthel H, Hamer K, Mulder J, van Es JH, de Koning E, Vries RG, Heimberg H, Clevers H. Unlimited in vitro expansion of adult bi-potent pancreas progenitors through the Lgr5/R-spondin axis. *EMBO J* 2013;32:2708–2721.
- Zuo X, Deguchi Y, Xu W, Liu Y, Li HS, Wei D, Tian R, Chen W, Xu M, Yang Y, Gao S, Jaoude JC, Liu F, Chrieki SP, Moussalli MJ, Gagea M, Sebastian MM, Zheng X, Tan D, Broaddus R, Wang J, Ajami NJ, Swennes AG, Watowich SS, Shureiqi I. PPAR $\delta$  and interferon gamma promote transformation of gastric progenitor cells and tumorigenesis in mice. *Gastroenterology* 2019;157:163–178.
- Ji T, Takabayashi H, Mao M, Han X, Xue X, Brazil JC, Eaton KA, Shah YM, Todisco A. Regulation and function of bone morphogenetic protein signaling in colonic injury and inflammation. *Am J Physiol Gastrointest Liver Physiol* 2017;312:G24–G33.

14. Haruma K, Ito M. Review article: clinical significance of mucosal-protective agents: acid, inflammation, carcinogenesis and rebamipide. *Aliment Pharmacol Ther* 2003; 18(Suppl 1):153–159.
15. Mizokami Y, Oda K, Funao N, Nishimura A, Soen S, Kawai T, Ashida K, Sugano K. Vonoprazan prevents ulcer recurrence during long-term NSAID therapy: randomised, lansoprazole-controlled non-inferiority and single-blind extension study. *Gut* 2018; 67:1042–1051.
16. Sandborn WJ, Ferrante M, Bhandari BR, Berliba E, Feagan BG, Hibi T, Tuttle JL, Klekotka P, Friedrich S, Durante M, Morgan-Cox M, Laskowski J, Schmitz J, D'Haens GR. Efficacy and safety of mirikizumab in a randomized phase 2 study of patients with ulcerative colitis. *Gastroenterology* 2020; 158:537–549 e510.
17. Pan T, Liu J, Xu S, Yu Q, Wang H, Sun H, Wu J, Zhu Y, Zhou J, Zhu Y. ANKRD22, a novel tumor microenvironment-induced mitochondrial protein promotes metabolic reprogramming of colorectal cancer cells. *Theranostics* 2020;10:516–536.
18. Venner JM, Famulski KS, Badr D, Hidalgo LG, Chang J, Halloran PF. Molecular landscape of T cell-mediated rejection in human kidney transplants: prominence of CTLA4 and PD ligands. *Am J Transplant* 2014; 14:2565–2576.
19. Sigal M, Reines MDM, Mullerke S, Fischer C, Kapalczynska M, Berger H, Bakker ERM, Mollenkopf HJ, Rothenberg ME, Wiedenmann B, Sauer S, Meyer TF. R-spondin-3 induces secretory, antimicrobial Lgr5(+) cells in the stomach. *Nat Cell Biol* 2019;21:812–823.
20. Burclaff J, Willet SG, Saenz JB, Mills JC. Proliferation and differentiation of gastric mucous neck and chief cells during homeostasis and injury-induced metaplasia. *Gastroenterology* 2020;158:598–609 e595.
21. Matsuo J, Kimura S, Yamamura A, Koh CP, Hossain MZ, Heng DL, Kohu K, Voon DC, Hiai H, Unno M, So JB, Zhu F, Srivastava S, Teh M, Yeoh KG, Osato M, Ito Y. Identification of stem cells in the epithelium of the stomach corpus and antrum of mice. *Gastroenterology* 2017;152:218–231 e214.
22. Han S, Fink J, Jorg DJ, Lee E, Yum MK, Chatzeli L, Merker SR, Josserand M, Trendafilova T, Andersson-Rolf A, Dabrowska C, Kim H, Naumann R, Lee JH, Sasaki N, Mort RL, Basak O, Clevers H, Stange DE, Philpott A, Kim JK, Simons BD, Koo BK. Defining the identity and dynamics of adult gastric isthmus stem cells. *Cell Stem Cell* 2019;25:342–356.
23. Saenz JB, Mills JC. Acid and the basis for cellular plasticity and reprogramming in gastric repair and cancer. *Nat Rev Gastroenterol Hepatol* 2018;15:257–273.
24. Bartfeld S, Bayram T, van de Wetering M, Huch M, Begthel H, Kujala P, Vries R, Peters PJ, Clevers H. In vitro expansion of human gastric epithelial stem cells and their responses to bacterial infection. *Gastroenterology* 2015; 148:126–136 e126.
25. Kabiri Z, Greicius G, Zaribafzadeh H, Hemmerich A, Counter CM, Virshup DM. Wnt signaling suppresses MAPK-driven proliferation of intestinal stem cells. *J Clin Invest* 2018;128:3806–3812.
26. Kim MS, Lee KP, Yang D, Shin DM, Abramowitz J, Kiyonaka S, Birnbaumer L, Mori Y, Muallem S. Genetic and pharmacologic inhibition of the Ca<sup>2+</sup> influx channel TRPC3 protects secretory epithelia from Ca<sup>2+</sup>-dependent toxicity. *Gastroenterology* 2011; 140:2107–2115, 2115 e2101–2104.
27. Zhang Q, Raof M, Chen Y, Sumi Y, Sursal T, Junger W, Brohi K, Itagaki K, Hauser CJ. Circulating mitochondrial DAMPs cause inflammatory responses to injury. *Nature* 2010;464:104–107.
28. Liu JC, Liu J, Holmstrom KM, Menazza S, Parks RJ, Fergusson MM, Yu ZX, Springer DA, Halsey C, Liu C, Murphy E, Finkel T. MICU1 serves as a molecular gatekeeper to prevent in vivo mitochondrial calcium overload. *Cell Rep* 2016;16:1561–1573.
29. Westfall TA, Brimeyer R, Twedt J, Gladon J, Olberding A, Furutani-Seiki M, Slusarski DC. Wnt-5/ pipetail functions in vertebrate axis formation as a negative regulator of Wnt/beta-catenin activity. *J Cell Biol* 2003;162:889–898.
30. Hwang IR, Kodama T, Kikuchi S, Sakai K, Peterson LE, Graham DY, Yamaoka Y. Effect of interleukin 1 polymorphisms on gastric mucosal interleukin 1beta production in Helicobacter pylori infection. *Gastroenterology* 2002;123:1793–1803.
31. Di Paolo NC, Shayakhmetov DM. Interleukin 1alpha and the inflammatory process. *Nat Immunol* 2016; 17:906–913.
32. Dolmetsch RE, Xu K, Lewis RS. Calcium oscillations increase the efficiency and specificity of gene expression. *Nature* 1998;392:933–936.
33. Pham LV, Tamayo AT, Yoshimura LC, Lin-Lee YC, Ford RJ. Constitutive NF-kappaB and NFAT activation in aggressive B-cell lymphomas synergistically activates the CD154 gene and maintains lymphoma cell survival. *Blood* 2005;106:3940–3947.
34. Murray PJ, Allen JE, Biswas SK, Fisher EA, Gilroy DW, Goerdts S, Gordon S, Hamilton JA, Ivashkiv LB, Lawrence T, Locati M, Mantovani A, Martinez FO, Mege JL, Mosser DM, Natoli G, Saeij JP, Schultze JL, Shirey KA, Sica A, Suttles J, Udalova I, van Ginderachter JA, Vogel SN, Wynn TA. Macrophage activation and polarization: nomenclature and experimental guidelines. *Immunity* 2014; 41:14–20.
35. Gharib SA, McMahan RS, Eddy WE, Long ME, Parks WC, Aitken ML, Manicone AM. Transcriptional and functional diversity of human macrophage repolarization. *J Allergy Clin Immunol* 2019;143:1536–1548.
36. Shapouri-Moghaddam A, Mohammadian S, Vazini H, Taghadosi M, Esmaeili SA, Mardani F, Seifi B, Mohammadi A, Afshari JT, Sahebkar A. Macrophage plasticity, polarization, and function in health and disease. *J Cell Physiol* 2018;233:6425–6440.
37. Kvietyts PR, Twohig B, Danzell J, Specian RD. Ethanol-induced injury to the rat gastric mucosa. Role of neutrophils and xanthine oxidase-derived radicals. *Gastroenterology* 1990;98:909–920.

38. Qiu Y, Yang S, Pan T, Yu L, Liu J, Zhu Y, Wang H. ANKRD22 is involved in the progression of prostate cancer. *Oncol Lett* 2019;18:4106–4113.
39. Kawabata A, Nishikawa H, Saitoh H, Nakaya Y, Hiramatsu K, Kubo S, Nishida M, Kawao N, Kuroda R, Sekiguchi F, Kinoshita M, Kakehi K, Arizono N, Yamagishi H, Kawai K. A protective role of protease-activated receptor 1 in rat gastric mucosa. *Gastroenterology* 2004;126:208–219.
40. Song SH, Kim JE, Go J, Koh EK, Sung JE, Lee HA, Choi KM, Kim HD, Jung YS, Kim KS, Hwang DY. Comparison of the response using ICR mice derived from three different sources to ethanol/hydrochloric acid-induced gastric injury. *Lab Anim Res* 2016;32:56–64.
41. Lacy ER, Ito S. Microscopic analysis of ethanol damage to rat gastric mucosa after treatment with a prostaglandin. *Gastroenterology* 1982;83:619–625.
42. Laine L, Weinstein WM. Histology of alcoholic hemorrhagic "gastritis": a prospective evaluation. *Gastroenterology* 1988;94:1254–1262.
43. Sigal M, Logan CY, Kapalczynska M, Mollenkopf HJ, Berger H, Wiedenmann B, Nusse R, Amieva MR, Meyer TF. Stromal R-spondin orchestrates gastric epithelial stem cells and gland homeostasis. *Nature* 2017;548:451–455.

---

Received October 11, 2020. Accepted June 25, 2021.

#### Correspondence

Address correspondence to: Yongliang Zhu, PhD, Laboratory of Gastroenterology, Second Affiliated Hospital of Zhejiang University School of

Medicine, Hangzhou, Zhejiang 310009, China. e-mail: [ylzhu@zju.edu.cn](mailto:ylzhu@zju.edu.cn); or Zhenya Song, MD, Department of International Healthcare Center and General Medicine, Second Affiliated Hospital of Zhejiang University School of Medicine, Hangzhou, Zhejiang 310009, China. e-mail: [songzhenya@zju.edu.cn](mailto:songzhenya@zju.edu.cn); fax: (86)-571-87214404.

#### Acknowledgements

The authors acknowledge Xia Xu and Dr Jinghong Xu (Department of Pathology, Second Affiliated Hospital of Zhejiang University School of Medicine) for accurate pathologic evaluation, and Qi Dong (Cancer Institute of Zhejiang University) for excellent skills in confocal microscopy. The authors also thank Hongxiang Sun (College of Animal Sciences, Zhejiang University) for his kind gift of mouse RAW264.7 macrophages.

#### CRediT Authorship Contributions

Jingwen Liu, Doctoral candidate (Conceptualization: Equal; Data curation: Equal; Formal analysis: Equal; Methodology: Equal; Project administration: Equal; Software: Equal; Visualization: Equal; Writing – original draft: Equal; Writing – review & editing: Equal)

Jingni Wu, Doctoral candidate (Data curation: Equal; Methodology: Equal; Project administration: Equal; Software: Equal; Validation: Equal)

Rui Wang, Master Degree Candidate (Data curation: Equal; Supervision: Equal; Writing – review & editing: Equal)

Dandan Zhong, MD, PhD (Methodology: Supporting; Project administration: Supporting; Resources: Equal; Supervision: Equal)

Yiqing Qiu, MD (Resources: Supporting; Supervision: Supporting; Validation: Supporting)

Hongping Wang, MM (Project administration: Supporting; Resources: Supporting; Validation: Supporting)

Zhenya Song, MD (Funding acquisition: Equal; Resources: Equal; Supervision: Equal)

Yongliang Zhu, PhD (Conceptualization: Lead; Funding acquisition: Lead; Project administration: Lead; Resources: Lead; Supervision: Lead; Writing – original draft: Lead; Writing – review & editing: Lead)

#### Conflicts of interest

The authors disclose no conflicts.

#### Funding

This research is supported by grants from the National Science Foundation of China (81672898 and 81472723) and a grant from the Natural Science Foundation of Zhejiang Province (LY17H050009).